I R I D E

An **I**nterdisciplinary **R**esearch **I**nfrastructure based on **D**ual **E**lectron linac&laser

D. Alesini[1], M. P. Anania[1], M. Angelone[14], D. Babusci[1], A. Bacci[3], A. Balerna[1], M. Bellaveglia[1], M. Benfatto[1], R. Boni[1], R. Bonifacio[7], M. Boscolo[1], F. Bossi[1], B. Buonomo[1], M. Castellano[1], A. Castoldi[17], L. Catani[4], M. Cestelli-Guidi[1], E. Chiadroni[1], V. Chiarella[1], A. Cianchi[4], R. Cimino[1], F. Ciocci[14], A. Clozza[1], G. Colo'[3],C. Curceanu[1], S. Dabagov[1], G. Dattoli[14], P. De Felice[5], G. Delle Monache[1], D. Di Gioacchino[1], D. Di Giovenale[1], E. Di Palma[14], G. Di Pirro[1], A. Doria[14], U. Dosselli[1], A. Drago[1], A. Esposito[1], R. Faccini[2], M. Ferrario[1], G. P. Gallerano[14], A. Gallo[1], M. Gambaccini[11], C. Gatti[1], G. Gatti[1], A. Ghigo[1], L. Giannessi[14], F. Giorgianni[2], E. Giovenale[14], C. Guaraldo[1], R. Gunnella[8], S. Ivashyn[12], S. Loreti[5], S. Lupi[2], A. Marcelli[1], C. Mariani[16], M. Mattioli[2], G. Mazzitelli[1], P. Michelato[3], M. Migliorati[2], C. Milardi[1], E. Milotti[13], S. Morante[4], D. Moricciani[2], A. Mostacci[2], V. Muccifora[1], P. Musumeci[10], E. Pace[1], C. Pagani[3], V. Palmieri[6],L. Palumbo[2], M. Pedio[14], A. Perrone[9], A. Petralia[14], V. Petrillo[3], P. Pierini[3], A. Pietropaolo[14], M. Pillon[14], R. Pompili[4], C. Quaresima[15], L. Quintieri[5], J. V. Rau, C. Ronsivalle[14], J. B. Rosenzweig[10], A. A. Rossi[6], A. R. Rossi[3], E. Sabia[14], L. Serafini[3], D. Sertore[3], O. Shekhovtsova[12], I. Spassovsky[14], T. Spadaro[1], B. Spataro[1], V. Surrenti[14], A. Tenore[1], A. Torre[14], C. Vaccarezza[1], A. Vacchi[13], P. Valente[2], G. Venanzoni[1], S. Vescovi[1], F. Villa[1], N. Zema[15], M. Zobov[1].

(1) INFN-Laboratori Nazionali di Frascati
(2) INFN and Universita' di Roma"La Sapienza"
(3) INFN and Universita' di Milano
(4) INFN and Universita' di Roma"Tor Vergata"
(5) Istituto Nazionale di Metrologia delle Radiazioni Ionizzanti, ENEA C R Casaccia.
(6) INFN-Laboratori Nazionali di Legnaro
(7) INFN Universidade Federal da Paraiba, Brazil
(8) Universita' di Camerino
(9) INFN and Universita' del Salento
(10) UCLA, Los Angeles, USA
(11) INFN and Universita' di Ferrara
(12) ITP NSC KIPT, Kharkov, Ukraine
(13) INFN and Universita' di Trieste
(14) ENEA
(15) CNR
(16) CNISM and Universita' di Roma"La Sapienza"
(17) Politecnico di Milano and INFN-Mi

1. Introduction

We describe in this report a preliminary proposal of a new large infrastructure for fundamental and applied physics research. Conceived as an innovative and evolutionary tool also for multi-disciplinary investigations in a wide field of scientific, technological and industrial applications, it will be a high intensity "particle beams factory", based on a combination of a high duty cycle radio-frequency superconducting electron linac (SC RF LINAC) and of high energy lasers. It will be able to produce a high flux of electrons, photons (from infrared to γ-rays), neutrons, protons and eventually positrons, that will be available for a wide national and international scientific community interested to take profit of the most worldwide advanced particle and radiation sources.

We can foresee a large number of possible activities, among them:

- Science with Free Electron Lasers (FEL) from infrared to X-rays,
- Nuclear photonics with Compton back-scattering γ-rays sources,
- Fundamental physics investigations with low energy linear colliders
- Advanced Neutron sources by photo-production,
- Science with THz radiation sources,
- Physics with high power/intensity lasers,
- R&D on advanced accelerator concepts including plasma accelerators and polarized positron sources
- ILC technology implementation
- Detector development for X-ray FEL and Linear Colliders
- R&D in accelerator technology and industrial spin – off

The main feature of a SC linac relevant for our facility is the possibility to operate the machine in continuous (CW) or quasi-continuous wave (qCW) mode with high average beam power (>1 MW) and high average current (>300 μA). The CW or qCW choice, combined with a proper bunch distribution scheme, offers the most versatile solution to provide bunches to a number of different experiments, as could be envisaged in a multi-purpose facility.

Europe is in a strategic position in the SC RF technology, mainly due to the strong contribution of European countries to the TESLA Collaboration. In particular Italy is in a leading position, with knowledge and strong capabilities in the design, engineering and industrial realization of all the main component of a superconducting radiofrequency accelerator. INFN strongly participated since the early design stages through the final engineering and shares the know-how and has the recognized intellectual property of several main components (one of which is the cryo-module concept and its evolution).

The realization of a superconducting linac at the Tor Vergata site in close proximity to the LNF laboratories will allow INFN to consolidate a strong scientific, technological and industrial role in a competing international context both to deploy a national multi-purpose facility along the scientific applications discussed in the following sections, and

to prepare a strong role for the contribution to possible future large international HEP projects as the International Linear Collider.

2. Evolutionary facility layout

The backbone of the proposed facility is a superconducting high duty cycle electron linear accelerator, with the required 2 K cryogenic plant, based on the L-band standing wave RF (1.3 GHz) cavities, developed by the TESLA collaboration, which currently drive the FLASH FEL facility in DESY and which, with minimal improvements of the cryo-module cooling system, could be upgraded to CW or qCW operation.

The second core device of the facility is the high energy cryogenically cooled Yb:YAG Laser system operating in a chirped pulse amplification architecture followed by a frequency conversion stage to achieve 515 nm wavelength. This technology allowed achieving recently 1 J at 100 Hz in the picosecond regime with a bandwidth of 0.1%.

By using standing wave SC accelerating structures, that can accelerate beams in both longitudinal directions, one can see an attractive scheme based on two linacs operating at a maximum energy of 1.5 GeV each, when working in the collider mode, or used in cascade, as a single longer linac, to boost the electron energy up to 3 GeV for higher energy electron beam applications. In addition when operating in the collider mode both linacs may partially recover the electron kinetic energy of the beam leaving the opposite linac after the interaction, thus increasing the overall efficiency of the system and simplifying the beam dump design.

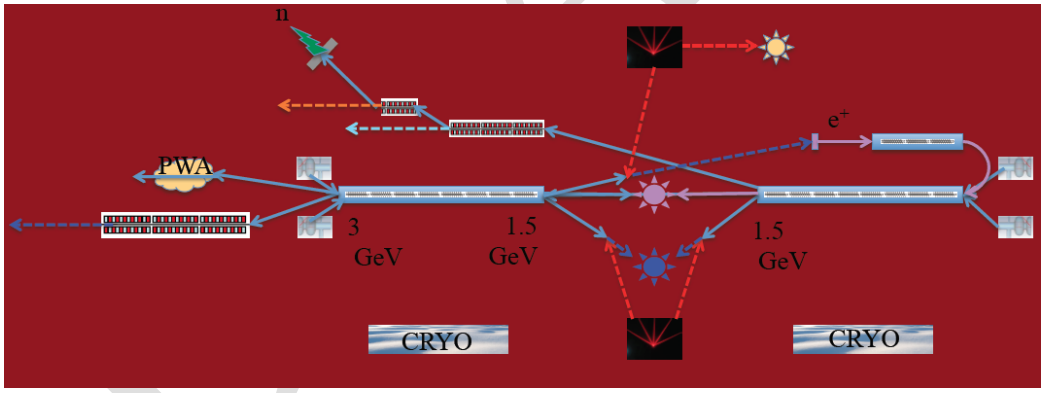

Figure 1: Schematic layout of the IRIDE accelerators and radiation sources complex

As indicated in Fig. 1 the 1.5 GeV linac system can drive FEL, Neutron and THz radiation sources and, in combination with the high energy laser, a γ-ray Compton source is also possible with many applications in the field of nuclear-photonics and as a possible tool for developing a polarized positron source as the one required for ILC.

With also the second linac installed one can envisage a low energy linear collider scheme for electron-photon, photon-photon and eventually electron-positron scattering studies. The combination of the two linacs, boosting the electrons up to 3 GeV, could also drive a short wavelength FEL user facility.

Advanced accelerators techniques could be also investigated. The success of the advanced accelerator activity as a vigorous and intense R&D program focused on the enabling technologies of plasma accelerators, Compton converters, gamma beam focusing, polarized positron source, superconducting RF gun and the associated advanced diagnostics instrumentation, could allow envisage a convenient energy upgrade of the facility to tens GeV level in a higher energy range of scientific applications.

3. The superconducting linac

The workhorse of the SRF technology is represented by the L-band (1.3 GHz) cavities [1] and modules, developed by the TESLA Collaboration [2,3], which currently drive the FLASH FEL facility in DESY and which form the main accelerator complex of the ~1.6 km European XFEL facility under construction, see Fig. 2. The TESLA/XFEL cavities and module concepts are well proven and understood and furthermore:

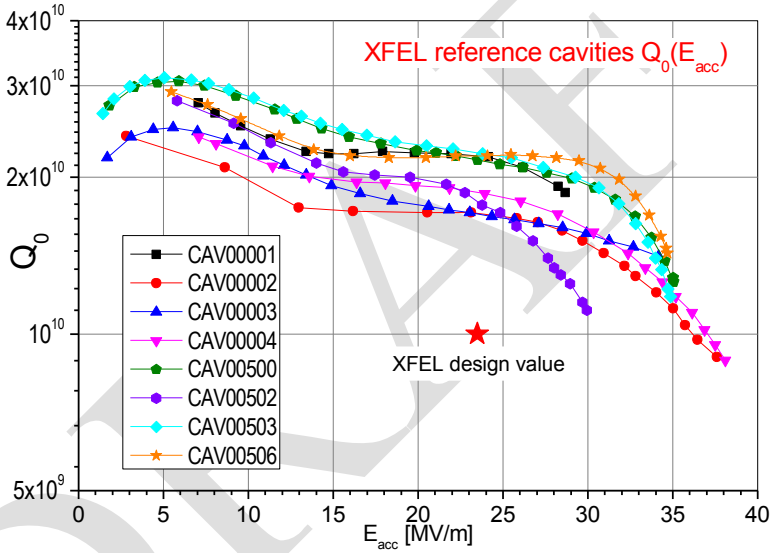

Figure 2: Test results of the cavities used for the qualification of the XFEL mechanical production infrastructure at the two vendors.

- Variations of the concepts for almost all components and subcomponents have been explored and tested for a variety of operating conditions (e.g. modified cavity and module geometries to deal with the larger heat loads associated to CW operation, longer modules to increase the real estate gradients, ERL configurations, etc.). The ILC S1-Global collaborative experiment at KEK proved that the concept can easily be adapted to the case of a combination of substantially different design variants for important components like cavities, tuners and couplers.
- A large industrial effort is currently ongoing in order to manufacture in Europe a large number of the European XFEL components (all 800 cavities, 50% of the ~100 cryomodules, all power couplers and RF stations). Half of the cavities and all the modules produced in Europe are procured in Italy, see Fig. 3. Industries have deployed large production facilities and infrastructures, taking over steps in the cavity

preparation process that were previously performed at research institutions (e.g. the needed surface treatments for the bulk niobium cavities to prepare them for operation). This capability and infrastructures exist and will contribute towards a potential decrease of the main accelerator components procurement costs and to rapid procurement times (the XFEL procurement reaches a cavity production rate of 4 cavities per week per vendor).

Figure 3: A set of pre-series XFEL cavities at the company E.Zanon.

Table 1 resumes the fundamental parameter and features for the state-of-the-art L-Band cavity and module technology.

Table 1: Main parameters or SRF L-Band components

Cavity	
Frequency	1300 MHz
Active length, L	1038 mm
Number of cells	9
Beam aperture	70 mm
R/Q	1036 Ohm
Geometric Factor	270 Ohm
Achieved gradient in vertical tests (electropolished), E_{acc}	>40 MV/m
Achieved operation in module conditions, E_{acc}	~35 MV/m
Achieved quality factor (Q_0) at design gradients	$> 10^{10}$
Cryomodule	
Number of cavities in module	8
Overall module slot (length + interconnection space)	12000 mm
Outer vessel diameter	965.2 mm (38”)

The choice of accelerating gradient for the superconducting linac cavities is strongly affected by the operating mode, time structure and current required to the beam.

High gradients in the 20-30+ MV/m range (needed to reach high energies) impose the choice of a pulsed beam structure at low (~ percent) RF duty cycle in order to limit power dissipation on the cavities, thus reducing the cryogenic requirements. RF pulses of ms

duration at ~10 Hz in the TESLA/XFEL cavities can deliver trains of thousands high-charge electron bunches (with ~MHz repetition within the RF pulses) to the experiments. The RF sources and RF distribution system need to provide the necessary RF power to the cavity through the main couplers in order to provide beam acceleration. Typically, klystrons with power rated in the MW range are used to feed simultaneously many cavities in a number of subsequent cryomodules. The following Fig. 4 and Tab. 2 illustrate the main relevant parameters for a model case, for a 1% duty cycle linac at 1 GeV.

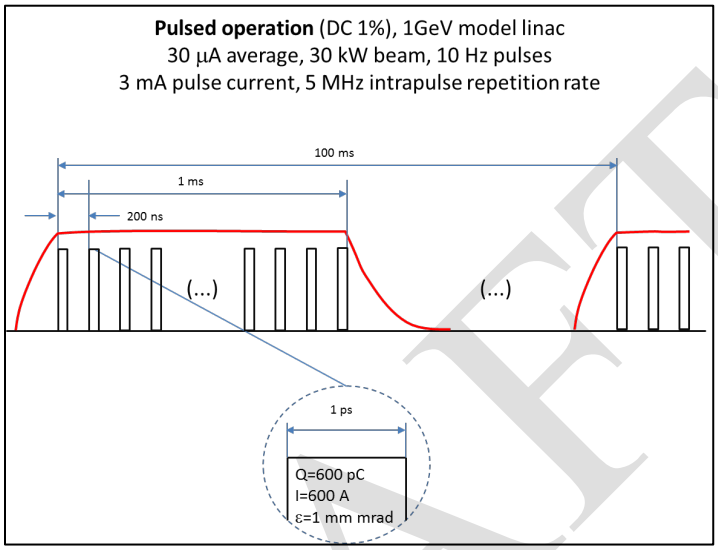

Figure 4: Typical time structure for pulsed operation .

Table 2: Relevant parameters for pulsed operation

1% duty cycle Model	
Beam parameters	
Beam energy	1 GeV
Beam average power	30 kW
Average beam current	30 uA
Average current in RF pulse	3 mA
Duty Cycle	1%
RF pulse length	1 ms
RF pulse repetition rate	10 Hz
Bunch Repetition within RF pulse	5 MHz
Number of bunches per RF pulse	5000
Charge per Bunch	600 pC
Bunch length	1 ps
Peak bunch current	600 A
Cavity and module parameters	
Cavity Accelerating gradient	25 MV/m
Average power per cavity	0.75 kW
Peak power per cavity	75 kW
Energy gain per module	200 MeV
Number of Cryomodules	5

Number of needed cavities	40
Linac overall parameters	
Linac Length	>60 m
Dynamic RF load at 2 K (no static)	0.024 kW

The SRF technology allows also to operate the accelerator in CW RF mode, delivering an uninterrupted train of moderate charge bunches at ~MHz repetition rates to the experimental areas. As RF dynamic losses on the cavity walls depend quadratically on the accelerating gradient, gradients need to be kept to moderate levels (~10 MV/m) to limit cryogenic consumption. Moderate power CW sources (IOTs or solid state transmitters in the few kW to tens of kW power range) can be used to power a single or few cavities. The Fig. 5 illustrate a model case in the parameter space, for a CW case at 1 GeV, see also Tab. 3.

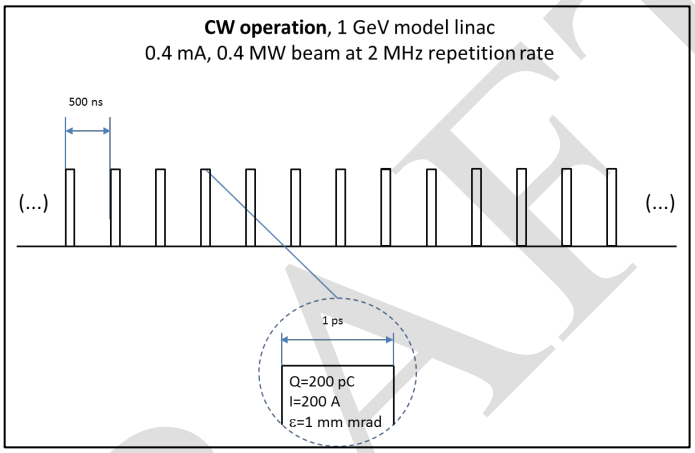

Figure 5: Typical time structure for CW operation .

Table 3: Relevant parameters for pulsed operation

CW Model case	
Beam parameters	
Beam energy	1 GeV
Beam power	0.4 MW
Average beam current	400 uA
Duty Cycle	100%
Bunch Repetition	2 MHz
Charge per Bunch	200 pC
Bunch length	1 ps
Peak bunch current	200 A
Cavity and module parameters	
Cavity Accelerating gradient	12.5 MV/m
Average power per cavity	5 kW
Energy gain per module	100 MeV
Number of Cryomodules	10
Number of needed cavities	80

Linac overall parameters	
Linac Length	>120 m
Dynamic RF load at 2 K (no static)	1.20 kW

These parameters are intended only to show the different possible scenarios for the linac parameter space as a guideline towards the finalization of a conceptual design meeting the combined requirements arising from the proposed experiments. The CW choice, combined with a bunch distribution scheme, offers the most versatile solution to provide bunches to a number of different experiments, as could be envisaged in the multipurpose facility.

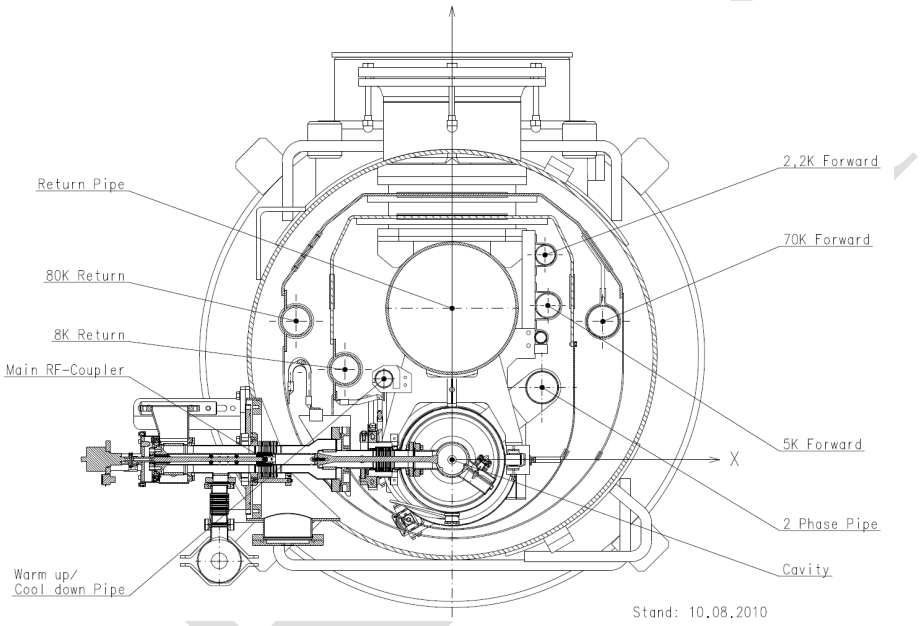

Figure 6: The TESLA/XFEL cryomodule transverse cross-section, showing the integration of the cryogenic lines.

The TESLA/XFEL cryomodule design is driven by the combined requirements of a good filling factor (in terms of ratio of nominal accelerating length with respect to the physical beamline length), moderate capital and operation costs (mainly focused on design simplicity and low static losses) and provisions for effective assembly and alignment of the beamline components. In this scheme the linac cryogenic lines are embedded in the cryomodules and strings of cryomodules are efficiently packed in strings of approximately 10-12 units fed by a single J-T supply valve able to provide the necessary low pressure 2 K helium for operation. A single standard LHC-unit cryoplant would be able to provide He for a ~2.5 km string of nearly 200 modules. These design requirements, originating from the linear collider application, imply that the concept, with few minor adaptations can serve both the scope of a high-gradient long linear accelerator at the percent duty cycle (as the case of the linear collider concept) and a short, moderate gradient facility delivering continuous (CW) beams. All piping is sized to provide minimal pressure drop in long (km size) circuits with low mass flow and can therefore be operated with larger mass flows for smaller lengths.

This versatility is demonstrated by the fact that the original TESLA Linear Collider concept has been chosen by XFEL (approximately 4% of the LC size), and is proposed for the CW schemes as the BESSY FEL, LBNL NGLS and even the Cornell ERL.
The adaptations required to fine tune the module concept to the operation mode concern mainly the cryogenic aspects:

- Set the frequency of LHe supply (J-T valves) in the string to provide the low pressure 2 K liquid He for the removal of the heat deposited by the RF accelerating field on the cavity walls.
- Review the cryo piping dimensions to ensure the correct pressure drop at the nominal mass flow in the cryogenic circuits, in order to provide the necessary temperature stability and flow conditions for safe cavity operation.

References:

[1] B. Aune et al., "Superconducting TESLA cavities", Phys. Rev. ST Accel. Beams 3, 092001
[2] TESLA TDR: http://tesla.desy.de/new_pages/TDR_CD/start.html
[3] ILC TDR: http://www.linearcollider.org/about/Publications/Reference-Design-Report

4. Laser systems

The laser system complex for IRIDE is one of its fundamental pillar, together with the electron accelerator complex and the experimental beamlines and detectors. As the electron accelerator is expected to provide a portfolio of advanced electron and positron beams of diverse performances, according to the specific experiment and/or beamline considered, the laser system complex is deputed to deliver optical photon beams able to fulfill the several requirements of the IRIDE facility. These can be categorized into three main areas:

A) drivers of photo-cathodes for electron beam generation at ultra high brightness, in the photo-injectors that will equip the IRIDE accelerator complex

B) colliding laser pulses to drive the back-scattering Thomson/Compton sources that will generate the advanced γ-beams of the IRIDE facility, that in turns will serve the several beam-lines of Nuclear Photonics and will drive the experimental clients like electron-γ or γ-γ colliders, as well as the positron source for the electron-positron collider and the one for test experiments on polarized positron beam production

C) drivers for high intensity plasma and vacuum advanced acceleration experiments, either to access extreme high gradient acceleration gradient, in excess of *TV/m* electric fields, and to access fundamental QED experiments of vacuum boiling also with coupling with the intense γ-beam produced by the Thomson/Compton sources

The crucial characteristic of laser systems in cathegory A is the capability to send on the photocathode surfaces a train of tens of UV laser pulses with controlled time-space intensity distribution in the sub-*ps* range, with nano-second spacing between successive pulses, carrying up to a few hundreds of microJoules of energy per pulse, synchronized at the sub-*ps* level with the RF of the linear accelerator, with a few percent stability in the energy per pulse as well sub-*ps* time-rise in the pulse time profile.

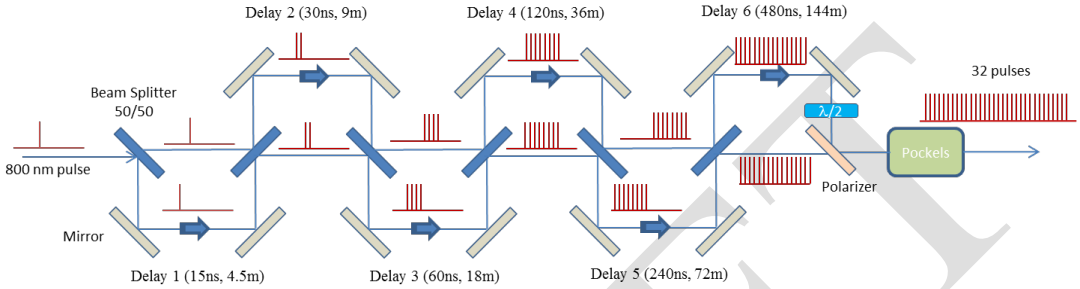

Scheme for 32 replica generation of UV Ti:Sa laser pulses to be sent to the photocathode

Laser systems in group B are characterized by high average power (100 *W*) with Joule-level laser pulses at high beam quality and picosecond pulses synchronized to the RF of the linear accelerator, together with extremely good stability in pointing (at the micro-radiant level) and very small bandwidths (less than 0.1%).

Group C lasers deliver the high intensity (10^{22} W/cm^2) peak power (1 *PW*) and ultra short (tens of femtoseconds) pulses needed to drive plasma waves in the LWFA scheme, to investigate high gradient laser-plasma advanced acceleration, and collisions of laser pulses with the γ-beams.

While laser systems in A and B are intrinsically coupled to the accelerator complex for the production of secondary beams (γ-beams and positrons), the laser system in group C is an ancillary device for additional experiments.

The best candidate for group A is a high rep rate (100 *Hz*) *Ti:Sa* laser system delivering 250 *mJ* in the IR with 3 *ps* FWHM pulses that can be splitted into a power of 2 pulse train to drive the photocathode (present ELI-NP design aims at 32 pulses in 600 *ns* pulse train). The cost of such a system, which is state of the art, is about 2 M€. For the *e-*γ or γ-γ colliders 2 of these systems will be necessary, in order to produce the two counter-propagating electron beams going to their respective Thomson/Compton interaction points.

The best candidate for laser system B) is definitely the *Yb:Yag* based on thin-disk technology: this was proved to be able to deliver 1 *Joule* pulses at 100 *Hz* rep rate, with high quality and *ps* long pulses. The cost foreseen for such a laser is about 6 M€: once again, 2 of these lasers are needed to drive the 2 colliding γ-beams for *e-*γ or γ-γ

colliders. The front-end of these laser, based on fiber lasers, is also suitable to pump a Fabry-Perot cavity for the production of γ-beams at very high flux, adequate for nuclear photonics experiments and applications.

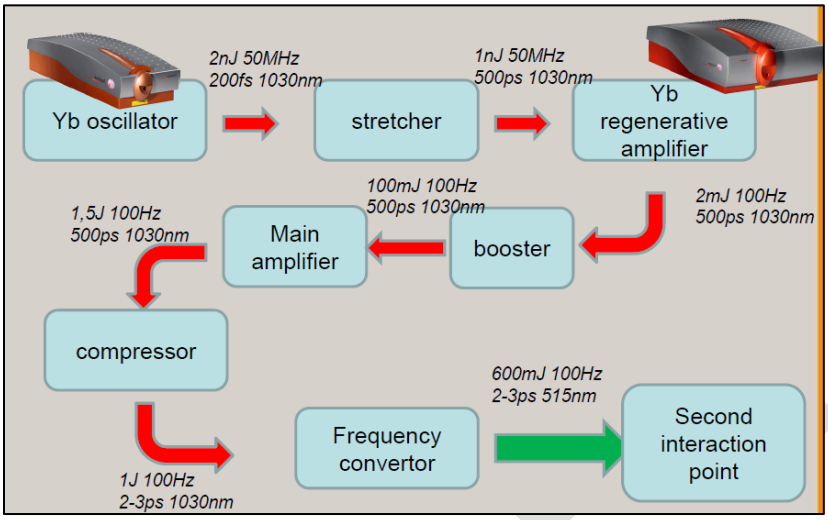

Functional drawing of the collision Yb:Yag laser system

According to other international projects in the field of high intensity lasers (BELLA, ELI), the *PW* laser system of group C is based on *fs Ti:Sa* lasers based on cryo-cooled *J*-level amplifiers at low rep rate (1-10 *Hz*), controlled by proper mazzler-dazzler schemes to ensure the large bandwidth spectrum control necessary to achieve high contrasts in the pre-pulse (up to 10^{10}). The cost of a similar system recently delivered to LBNL for the BELLA project, by a well known company, was about 10 M€.

5. Preliminary cost estimate of the facility

The complete cryo-module units, including cavities, couplers, magnet, RF source/distribution and LLRF controls, cold vacuum and assembly/installation operations, and the necessary cryo-plant represent the cost driver for the accelerator complex components. A rough estimate for the SC linac capital costs has been based on the European XFEL experience and CERN scaling laws of cryo-plants and is presented in the following tables.

By its nature the deployment of a linac can be done stepwise with increasing final electron beam energy. One can foresee for example an installation and investment strategy with at least 2 evolutionary configurations with different applications:

Step 1 *– with only one 1.5 GeV linac operating in the CW mode coupled to the high energy laser, allowing the following applications:*

- Free Electron laser oscillator
- γ-rays source by Compton back-scattering

- Nuclear photonics
- Polarized positron source development
- Neutron source,
- THz radiation source,
- Advanced accelerator concepts experiments

as illustrated in the following scheme:

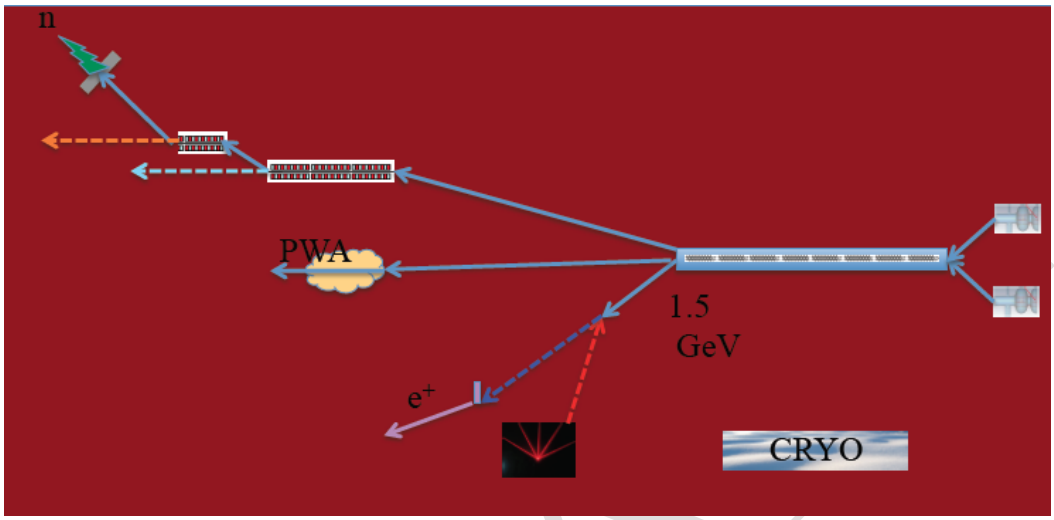

Figure 7: Schematic layout of the IRIDE complex, step 1

which requires an initial investment summarized in Tab. 4:

Table 4: Cost estimate for step 1

Components	**M€**
Injector 1	10
Linac 1 modules including CW RF	30
Cryogenic Plant 1	20
Total for Linac 1	**60**
FEL undulators	10
FEL Optics and user beam lines	20
Total for FEL	**30**
Neutron source	**5**
Advanced Accelerator Exp.	**5**
THz source	**3**
C-band Injector	13
High Energy Yb:YAG Laser 1	7
Interaction region and laser recirculator:	4
γ-ray beam collimation and diagnostics	3

Compton Users Beam Lines	10
Total for Compton source	**37**
Polarized positron source	**5**
GRAND TOTAL	**145**

Step 2 *– with two 1.5+1.5 GeV linacs coupled with the high energy laser which can operates in two different modes:*

- *Higer energy mode up to 3 GeV for:*
  - short wavelength Free Electron Laser

- *Collider Modes for :*
  - $e^- \gamma$ collisions for the precise measurement of the π^0 width through the process $e^- \gamma \rightarrow \pi^0 e^-$ (Primakoff effect),
  - $\gamma \gamma$ collisions for fundamental studies on QED, for example to observe and measure photon-photon scattering,
  - $e^+ e^-$ collision experiments up to 3 GeV energy in the center of mass

as illustrated in Fig. 1 and with the additional investment summarized in Tab. 5

Table 5: Cost estimate for step 2

Components	**M€**
Injector 2	10
Linac 2 modules including RF	30
Cryogenic Plant 2	20
Total for Linac 2	**60**
FEL undulators	20
FEL Optics and user beam lines	40
Total for FEL	**60**
High Energy Yb:YAG Laser 2	7
Detector e/γ γ/γ	10
Total for e/γ γ/γ collider	**17**
Positron surce	
Damping Ring ?	
Detector e^+e^-	
Total for e^+e^- collider	**To be evaluated**
GRAND TOTAL	**137**

Some additional components are required to operate each facility configuration listed above. More than one electron injector will be certainly adopted in order to provide the specific beam temporal structure, being a full CW electron injector with the required flexibility not yet available. FEL undulators, optical transport lines for FEL and Compton users, large detectors for particles and photons experiments, neutron target and other

components shown in the figure will be described in a more detailed report. Last but not least one has to consider the impact on the overall cost of the buildings and the infrastructure services that will be evaluated when a more precise machine layout will be available.

6. Overview of scientific cases

6.1. Free Electron Lasers

Photons are the most important probe to investigate our environment. From radio frequencies to hard X-ray photons are used since many years to get both electronic and structural information on virtually any materials, form biology to condensed matter systems. Among the different types of sources, storage rings to emit Synchrotron Radiation (SR) have a special place because of the capability to produce radiation with very high flux and brightness in an energy range from infrared to hard X-ray. The development of storage rings with special magnetic components over the past thirty years has led to third generation machines, especially designed for SR research, with the peculiarity to have radiation with unprecedented degree of brilliance. This important property makes possible to routinely perform experiments which were previously only conceivable, like X-ray diffraction (XRD) from surfaces, huge biological molecules or magnetically ordered structures. In parallel, new experimental techniques like X-ray absorption spectroscopy (XAS), which allows measuring the local structural and electronic properties of matter or inelastic X-ray scattering, to probe the lattice dynamics in solids, were developed. Today, in the SR facilities thousands of researchers, coming from many different countries perform their experiments, contributing to the advance of scientific knowledge in many different fields and bridging the traditional dichotomy between applications and fundamental science.

The Free Electron Laser, allow to generate coherent radiation in the X-ray energy domain with optical properties similar to the conventional lasers [1,2]. The X-ray FEL has the possibility to generate X-ray beams with a peak brilliance of several orders of magnitude higher than the third generation SR sources. It also offers an extremely short pulse length, typically in the femtosecond time domain with some degree of tunability and a high degree of either linear or circular polarization. The possibility of operating a FEL with a superconducting (SC) LINAC offers significant advantages in terms of flexibility and opens new possibilities for large scale facilities, employing fourth generation synchrotron radiation sources. The first operating FEL exploited the Stanford SC LINAC as electron beam source , being at the time the most reliable accelerator in terms of beam qualities, RF bunch structure and stability. The choice of more conventional accelerators in the subsequent development of the FEL devices was dictated by the intrinsic complexity of the underlying technology and by the relevant high cost of operation. The technological evolution, occurred since the seventies of the last century, has significantly reduced the costs and the operating conditions of a SC accelerating device. The use of a SC LINAC would offer a significant breakthrough for short wavelength FEL oscillators, would increase the average power of fourth generation synchrotron radiation sources and increase the relevant capabilities in terms of users.

The natural time, energy and length scales of the physical processes span an enormous range of about fifteen orders of magnitude, depending on the atomic, electronic, spin structure and some other parameters. To have a visual insight of the typical magnitude scales at the atomic level we report in Fig. 8a the characteristic time, energy and length involved in the atomic interactions. The aim is to drive the choice of the best architecture of a FEL device to be a large scale facility with the highest degree of flexibility and applications. The challenge is therefore that of developing a flexible enough source capable of probing the matter with finer length, time and energy resolution, where biological systems can be observed on their femto-(atto-)second temporal, nanometers spatial and milli-electronvolts energetic scales. Dynamic studies are the future of the research, complementing the investigation of static systems. To reach these goals, the next generation of light sources should have elevated transverse and temporal coherence, pulse duration of femtoseconds and possibly attoseconds, high brilliance and peak and average power, rapid and broad range tunability of photon energy and full polarization control. Free Electron Lasers has been viewed as a unique device to achieve these goals.

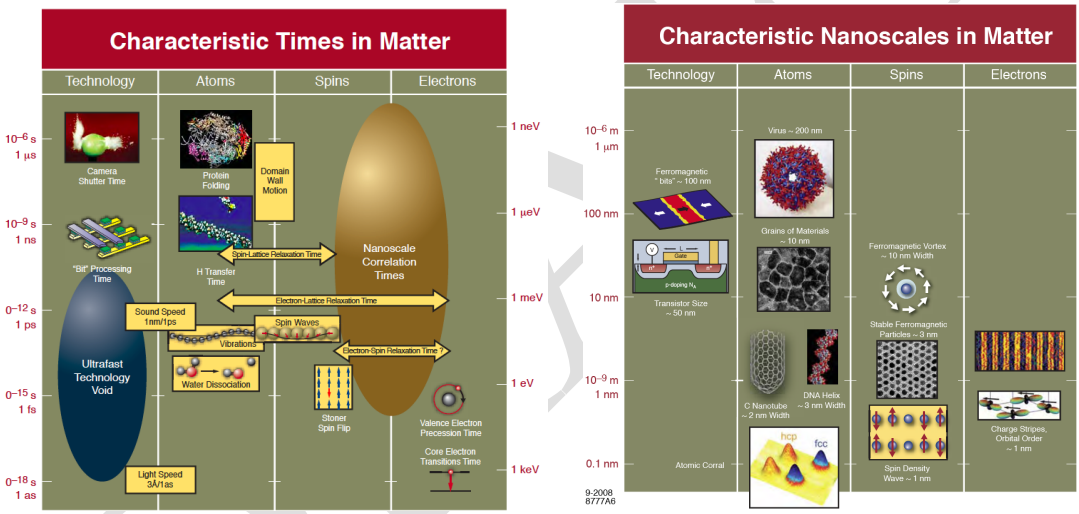

Figure 8a: Left: Illustration of the present knowledge on typical time and energies involved in the interactions of atoms, electrons, and spins. Right: Typical scale length involved in the study of nano-world

The problem of conceiving the design of a FEL device capable of providing all the needs summarized in Figs. 8a is a very challenging since it would require an effort aimed at combining different aspects of FEL technology ranging from oscillators, to SASE, to SEEDED and SELF SEEDED configurations. A not secondary challenge would be the possibility of driving the various FEL components with an e-beam driven by the same accelerators, thus automatically satisfying all the issues associated with time synchronization, necessary to exploit the different laser beams in e. g. pump and probe experiments. Furthermore a FEL source with such a flexibility should allocate part of its time to experiments aimed at testing fundamental problems in electrodynamics and to develop new schemes for FEL operation.

The FEL emission at wavelengths ranging from 0.3 to 10 nm at fundamental harmonics, allowing also the achievement of the 1 Å region using the third and fifth harmonics, open possibilities for novel methodologies based on X-rays imaging and on time-resolved studies in material science, in biology and in medicine, along with many applications of non-linear optics. The FEL source will furthermore allow to send a huge energy concentration on small areas of condensed systems. This will make it possible the discovery of new phenomena, which cannot be forecast through a simple extrapolation of what already known at present.

Looking to the biological applications we start from the basic consideration that the knowledge of the 3D structure of proteins and macromolecules is crucial to understand their biological functions at the molecular level. At the present time XRD is the main technique to get detailed structural information with atomic resolution. This method needs photon beam with wavelength of the order of 1 Å and crystals of suitable quality and size. In the modern SR facilities diffraction data are routinely measured on crystals of the size of 10-100 μm using micro-focus beam-lines. However, the problem of growing high-quality crystals is the major drawback for many proteins, especially those with a high predominance of hydrophobic interactions, like for example membrane proteins, or large protein complexes. On the other side it should be recalled that very small crystals are easier to grow than large ones, most of the time the crystallization trials produces crystals of extremely small size, typically of the order of 100 nm edge. The measurement of such samples is outside the capability of any micro focus beam line in the SR facilities. The X-ray FEL promise to solve this problem because the unprecedented high x-ray fluence provides a sufficiently large number of photons to enable structure determination from diffraction measurements of streams of nano-crystals and even single molecules. However, due to an extremely high fluence that is about 100 times larger than the conventional damage limit samples are subject to severe radiation damage. The ultra-short x-ray pulses generated by x-ray FEL enable us to carry out ‘‘diffraction before destruction’’ within femtosecond time scales to suppress nuclear motion. Recently the first experiment of this type has been done at LCLS-FEL facility getting diffraction pattern from a large photosystem membrane complex that crystallizes in samples of about 250 nm size corresponding at seven unit cells. In Fig. 8b we report the diffraction pattern and the electronic density reconstruction of this membrane complex obtained with a 80 fs pulse duration [5].

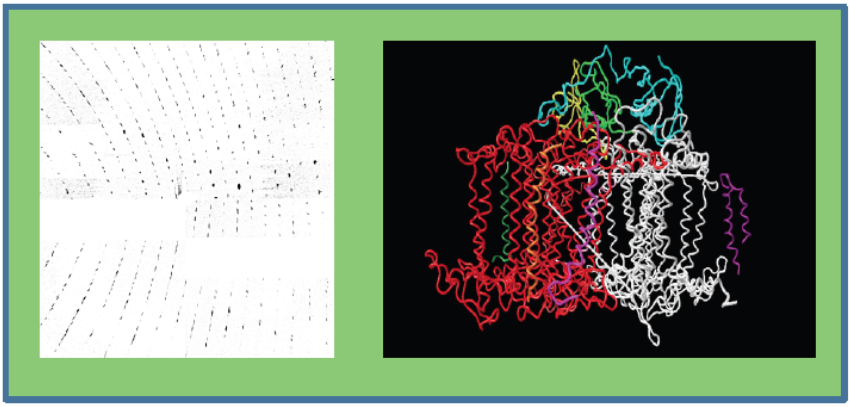

Figure 8b Left: diffraction pattern of the Photosystem I complex measured at LCLS with a photon beam of 1.8 KeV and a time length of 80 fs. Right: Electronic density reconstruction at 7Å of structural resolution.

The use of the Soft X-rays we allow to bridge the gap between the experimental resolution reachable by light microscopy in the visible, which yields insight on the gross structural organization of the cell and its organelles, and the atomic resolution provided by hard X-ray techniques. In the wavelength region between the K-absorption edges of oxygen and carbon, i.e. in the so-called "water window", which lies around 2.7 nm where the absorption by organic carbon and nitrogen containing material is much higher than that by oxygen, imaging spectroscopy can be carried out on biological specimens up to about 10 μm-thick. This means that the whole cell can be imaged in an aqueous environment close to its native state. A FEL tuned in the wavelength energy range 13-1 nm make the possibility to perform Soft-Xray microscopy with either high spatial resolution, yielding sub-nanometer structural information, or with high energy resolution, providing detailed chemical information, or both, thus opening the way for a wealth of new biological experiments. Concretely X-ray microscopy offers the possibility of performing a number of important experimental investigations on topics of great biological interest like, for example, diffusion processes of small molecules in biological membranes, monitoring of protein folding and protein aggregation in living cells, monitoring of molecular events induced by the presence of drugs.

Typically time dependent experiments are done by a pump and probe scheme. Here a pump mechanism, which excites the system, is synchronized with a probe that observes its evolution; the application of this method provided extremely valuable results in the spectroscopic study of molecules, liquids and solids. The possibility of having femtosecond X-ray pulses allows to monitor and measure in a direct way the structural changes occurring in a system when in a short lived excited state generated by such mechanism. These structural changes are due to a charge redistribution in the excited state and can be probed by using time-dependent XAS and scattering techniques. Experiments which illustrate the great opportunities for structural studies in the areas of molecular photochemistry and in the study of electron – lattice coupling in solids have been recently reported using storage rings based synchrotron radiation sources. They have been made in the several tens of ps time domain and are only suggestive of the kind of science which will be possible in the near future with the fully availability of X-ray free electron lasers; these new sources promise to provide a great impetus to this field in view of the reduced pulse duration and the extremely high photon flux per pulse. The common basis to these investigations are the characteristic time scales involved in the photo-excitation process (< 1 fs), in atomic vibrations (10 – 100 fs) and that of the electron – phonon interaction time (~ 1 ps).

In photochemical and photo-biological reactions, photon absorption leads to redistribution of electrons in valence states and thus to breaking and formation of bonds, the initial steps of chemical activity and biological function. The possibility of using as probe the X-rays allows to study in real time the geometric changes accompanying photo-excitation using both fast XAS and XRD and photoemission.

The understanding of the properties of condensed matter is based upon the separation of vibrational and electronic degrees of freedom in the framework of the Born

– Oppenheimer approximation. However, there are cases in which the interaction between the lattice and the electrons is strong, leading to intriguing phenomena such as superconductivity, metal – insulator transitions and colossal magneto-resistance, for example. Probing the lattice – electron coupling is of great importance in these systems. One of the most promising approaches to do so consists in altering the population of electronic states by photo-excitation using a fs laser pump and subsequently probing the structural changes with fast X-ray diffraction.

The advent of VUV and x-ray FELs has opened the way to investigation of the interaction of matter with high intensity, ionizing radiation: previously high field light sources were limited to low photon energies. Some of the first targets to be investigated were clusters, particularly noble gases. The physics of the interaction of high intensity light with this form of matter is different from that of optical laser-matter interaction, and is a field of broad interest ranging from a fundamental understanding of ionization dynamics and plasma formation to consequences for x-ray imaging. The possibility of creating and studying matter at extreme conditions open the way to look to key process at work in extreme plasmas like those found in stars, the rims of black holes and other massive cosmic phenomena. Most astrophysical objects emit X-rays, produced by highly charged particles in superhot gases or other extreme environments. To model and analyze the extreme forces and conditions that generate those emissions, scientists use a combination of computer simulations and observations from space telescopes. Recently the Fe16+, an iron nucleus with only 10 orbiting electron, as opposed to the usual 26, has been created and measured at LCLC-FEL facility. This ion is of particular interest because it produces some of the brightest cosmic X ray signals. But satellite measurements show those signals are more than 30 percent dimmer than leading theories predict. The analysis done in this study shows that the problem lies in our ability to model the structure of the ions, indicating the need to substantially improve our theoretical description of the matter at extreme conditions. Such measurements conducted at FEL will be important for interpreting X-ray emissions from a plethora of sources, including black holes, X-ray binaries, stellar coronae and supernova remnants, to name a few [6].

Our FEL project will be designed to make the above quoted experiments. At the beginning two beam lines will be constructed to maximize the user's accessibility, one will be optimized to make imaging experiments and the second to perform time dependent spectroscopies from core-levels like XAS and photoemission. This last is quite demanding both for the machine and beam line designs because of the energy tuning of the photon beam, of the order of 15-20 % of the nominal energy, and the need to preserve the time length of the FEL pulse even in the presence of a sufficient photon energy resolution.

Beam lines in a FEL facility are characterized by their length, typically of the order of 100 meters for energies in the X-ray domain. Several physical reasons make such length compulsory: the scarce reflectivity of all optical elements for photons in the KeV energy range, the need of spatial separation of the FEL radiation direction from the Bremsstrahlung γ radiation beam generated inside the undulator by the interaction of highly energetic electrons with the residual gas, the requirement to concentrate the FEL radiation in few tens of nm2 to perform many experiment such as nano-metric imaging,

single shot scattering on macromolecules and so on. In a 100 meters long beam-line this can be simply achieved with a proper choose of the magnification ratio.

Two beam lines are considered in the first phase of the IRIDE project, thought to maximize the user's accessibility. The first will be optimized for imaging experiments while the second to perform time dependent spectroscopy from core-levels preserving the time length of the FEL pulse.

The concept of the free electron laser line is such that it provides either a FEL facility and a complement to the architecture of the LAB. The various components are listed below and sketched in Fig. 9.

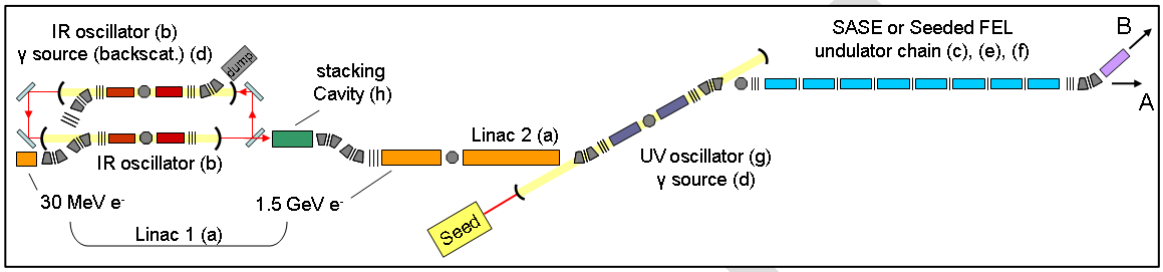

Figure 9: FEL beam lines architecture

a) Two S-C-LINACS with 1.5 GeV maximum energy
b) Between the two Linacs a double FEL oscillator, with a manifold role, is inserted
c) The undulator chain can be powered by the beam operating at full energy (3-GeV) or less
d) A second FEL oscillator is added for the operation in the UV region and for intra-cavity backscattering for the realization of a gamma source to be exploited for Nuclear Physics studies and the production of polarized electrons
e) The third FEL section may operate in SASE or SEDEED mode
f) The seeding will be achieved by exploiting a conventional seeding procedure or by using the self- seeding scheme based on a kind of oscillator-amplifier device, according to the scheme developed in [3,4]
g) An oscillator with mirrors at $13.5\,nm$ can eventually be considered for the operation at short wavelength seeding

The realization of the whole device should be considered evolutionary and each step should provide a well-defined item with a well-specified application. The SC LINAC sections can be developed along with the Infra-LINAC FEL, whose role is strategic for the rest of the facility. The two sections may also be operated with a low number of accelerating cavities to produce a beam with the energy necessary for the realization of an IR-FEL and for QED test.

The second oscillator in the UV can be operated when the LINACs are not at the full energy, and the performances of the first oscillator as beam heater can be tested.

The construction of the undulators can be undertaken in parallel to that of the accelerators, and techniques of beam sharing on different undulator lines can be tested. Two "parallel" FEL oscillators can be constructed by using different portion of the e-beam, as shown in Fig. 9, the lasers, if operating at closer frequencies, can be exploited for two colors experiments.

Table 6 summarizes the different evolutionary steps, each step demands for a substantive effort of R&D and evolves towards increasing levels of complexities, which should be carefully controlled to make the facility reliable.

Table 6: summary of expected FEL performances

Electron beam energy	FEL osc_I	FEL osc_II	FEL osc_III	SASE&Seeding
50-100 MeV	10-0.1 X-ray intracavity generation			
750 Mev		120 nm+ Harmonics& Intracavity-scattering		30nm-10nm
2.28 GeV			13.5nm+ Harmonics &intracavity scattering	6-2 nm
3 GeV				1-0.1nm

This effort requires a strong support and collaboration by industries in particular by those operating in the mechanical and of control electronics sectors. Further support from sectors developing material science is required in particular from those operating in the production and manufacturing of magnets and of high performances optics. Such an effort might provide a significant impact for the researches in this field and to open new possibilities in the relevant technologies.

References:

[1] W.A. Barletta et al., "Free electron lasers: present status and future challenges", NIM-A 618 (2010).

[2] G. Dattoli, A. Renieri and A. Torre, Lectures on Free Electron Laser Theory and Related Topics, World Scientific Singapore (1995)

[3] F. Ciocci, G. Dattoli, A. Torre and A. Renieri, Insertion devices for Synchrotron radiation and Free Electron Laser, World Scientific Singapore (2000).

[4]G. Dattoli and P. L. Ottaviani, J. Appl. Phys. 86, 5331 (1999)

F. Ciocci et al. IEEE-JQE 31, 1242 (1995).

[5] Chapman et al. Nature 470, p.73 (2011)].

[6] S. Bernitt et al. Nature 492, pag. 225, (2012)].

6.2. R&D on X-ray detectors

The scientific activities foreseen at IRIDE lead to specific and challenging requirements with respect to x-ray instrumentation and in particular to x-ray detectors. These requirements ask for detectors that cover a wide energy range, from soft to hard x-ray energies, with specification in some cases exceeding the existing technology. It is clear that a successful exploitation of the unprecedented features of the x-ray radiation that will be available at IRIDE calls for a dedicated and substantial detector R&D program which also opens the opportunity to enhance the Italian scientific and technological leadership as well as the international links in this cutting-edge field.

The parameters of the FEL X-ray source at IRIDE have direct consequences on the detectors to be used in the experiments. First of all the wide energy range of the x-rays - from few tens of eV up to about 12 keV (corresponding to wavelengths ranging from 0.1 nm to 30 nm) - cannot be covered by a single detector or by a single technology but different detection systems optimized for a limited energy range need to be developed. As an example, in case silicon is used as the detecting material (direct detection), at X-ray energies below 700 eV the attenuation length becomes so small (<1 μm) that the entrance window for radiation on the detector surface has to be specially fabricated in order to minimize photon absorption in the insensitive surface layer. Moving towards higher X-ray energies the problem of the entrance window is no more a critical point but detection efficiency starts dropping (e.g. below 90% at 10 keV for a 300 μm thick silicon wafer) and radiation hardness of the interfaces on the opposite detector surface or of the ASIC may become an issue. The Compton source will deliver even harder X-rays, covering a wide spectrum above 100 keV that will therefore require the investigation of high Z materials or of X-ray conversion in scintillator crystals in suitable arrangements in order to achieve acceptable quantum efficiencies.

A specific challenge for detector development at IRIDE, as compared to other FEL sources, is in the time structure of the X-ray beam. As every X-ray pulse can be regarded as a new imaging experiment, the imaging detector must be able to readout, digitize and store the data before the arrival of the next pulse. As a reference, the Linear Coherent Light Source (LCLS) in US, the Spring-8 Compact SASE source (SCSS) in Japan or FERMI@Elettra in Italy, using non-superconducting accelerator technology, currently feature evenly spaced pulses at rates from 120 Hz to 10 Hz respectively - a non-critical operating condition for state-of-the-art detection systems. The European XFEL at Hamburg is able to produce much higher average pulse rate, of about 30,000 pulses per second, but these pulses are delivered in bunch trains of about 3,000 pulses with a very challenging time separation of 220 ns only but followed by a long silent gap (99.4 ms) which can be used to perform off-chip data transfer unfeasible during the bunch train. At IRIDE the CW operation of the LINAC will provide evenly spaced pulses at a rate of 2 MHz - providing nearly two orders of magnitude more luminosity than the European XFEL – but leaves only 500 ns to readout each frame without any time gap.

Although every experiment may require a specific detection system, we may reduce the analysis to the ones required by the two major scientific cases: detectors for spectroscopy and detectors for imaging experiments. Time-resolved spectroscopy experiments will typically require energy-dispersive detectors with state-of-the-art energy resolution with possible position sensitivity for angular-dispersive experiments. The main challenges are the energy resolution, the quantum efficiency in the considered energy range and the

expected photon rate, as conventional energy-dispersive detectors may suffer from excessive pile-up. Therefore also new and dedicated signal processing electronics must be developed to overcome these limitations. Silicon Drift Detectors (SDD) optimized for X–ray spectroscopy is the leading technology that proved Fano-limited energy resolution, high count rate capability (up to MHz) and a quantum efficiency allowing operation from 100 eV to 10 keV [1]. High Z materials offer larger efficiencies than silicon and can extend the sensitivity to the harder X-ray spectrum. As they do not feature a native oxide layer they should also be extremely radiation hard in a high X-ray flux environment. Cryogenic detectors can achieve one order of magnitude better higher energy resolution than semiconductor detectors. For their exceptional energy-resolution they have been already employed at synchrotron facilities for X-Ray Fluorescence (XRF) and fluorescence-detected X-ray Absorption Spectroscopy (XAS) though the limited count rate may limit their applicability [2].

Imaging experiments will require 2D detectors as baseline detectors which demand novel developments. In this case the available peak brilliance of the x-rays will result in a large dynamic range at every detector element yet the detector must be able to discriminate the difference between zero and one photon (single photon sensitivity) in the low intensity regions.

Another issue is the signal generated per absorbed photon. In silicon, direct detection of a 50 eV photon will generate 14 electron-hole pairs which requires an exceptionally low noise performance of the system therefore investigation on avalanche multiplication structures and/or peculiar readout strategies in order to achieve single photon sensitivity should be evaluated. A 12 keV photon will instead generate 3315 electron-hole pairs which instead poses a major limitation to the useable dynamic range and to the required full well capacity. Moreover such high local photon rate on the detector will produce a very high level of charge generation in the detector, leading to the known formation of a local electron-hole plasma which impacts on the charge collection process, more significantly for the higher energy X-rays. This effect should be carefully taken into account as it broadens signal image with respect to the incident photon distribution and increases collection times.

A non-exhaustive list of state-of-the-art 2D imaging detectors and technologies, either available or in the development phase, should include charge-coupled devices (CCD), linear silicon drift detectors (LSDD), hybrid pixel detectors (HPD), monolithic active pixel sensors (MAPS). Some examples are given in the following.

The CAMP chamber, developed by the Max Planck Advanced Study Group to meet the challenge of novel VUV and X-ray FEL sources, houses the world's largest pn-CCD chips. These pn-CCDs operate with a frame readout rate of up to 200 Hz and are thus fully capable of meeting the requirements at LCLS (up to 120 Hz) and SCSS (up to 60 Hz). The pn-CCD of the CAMP camera is built on fully-depleted high resistivity silicon and features a voxel size of 75 x 75 μm^2 and a read-out noise of 2.5 electrons (rms) at an operating temperature of -50°C [3].

The Linear Collider Flavour Identification collaboration has developed MOS-CCDs with fast column parallel readout, bump-bonded to the readout ASIC, which can provide a pixel size of 20 μm or even smaller and aim at a fast readout frequency (50 MHz). It has also demonstrated the concept of the In-situ Image Storage Sensor (ISIS), a CCD in which signals are stored in-pixel during a burst train and can be read out in the inter-burst

gap. Similar pixel size is obtained with conventional MOS-CCDs, capable of high-speed readout due to multiple output ports, fabricated on thick, high-resistivity silicon with tailored entrance window providing simultaneously optical sensitivity with excellent blue and red quantum efficiencies, sensitivity to X rays from the VUV to 10 keV, and to low energy electrons [4].

Linear silicon drift detector architectures for position sensing and X-ray spectroscopy allow combining a fast readout speed, by continuously drifting the charges along the column by an electrostatic field, with very low noise leading to excellent spectroscopic performance. By keeping drift lengths below 1 cm, frame rates of 1 MHz can in principle be achieved. The drift detector principle for position sensing has been implemented several times in detectors for high-energy physics as well as for space research and can be designed in large areas. The design implements suppression of inter-column broadening of high signal charges and on-detector integrated electronics to reach low-noise spectroscopic performance [5].

To fulfill the challenge of the fast burst mode (up to 4.5 MHz burst frequency) and of the large dynamic range the European XFEL launched a call for proposals for 2D detectors and three projects are currently under development [6]. The Adaptive Gain Integrating Pixel Detector (AGIPD) is a classic silicon pixel array bump-bonded to the CMOS ASIC mainly targeted to imaging applications at 12keV [7]. The ASIC design uses dynamic gain switching to cover the large dynamic range combined with an analogue pipeline to store the recorded frames during the 0.6 ms-long bunch train, that are subsequently digitized and stored during the 99.4 ms gap. The design goal for the ASIC is 200 µm x 200 µm pixels containing more than 200 storage capacitors. The Large Pixel Detector (LPD) [8] attempts to cover the large dynamic range by implementing three different gain settings in parallel, each followed by an analogue pipeline with 500 storage cells per pixel which leads to larger pixel size of 500 µm. The DePMOS Sensor with Signal Compression (DSSC) is one of the few HPD developments addressing the low energy range (<6 keV) [9]. DSSC uses analog signal compression in the active pixel to accommodate the high dynamic range thanks to a specially designed non-linear response of the DePMOS transistor embedded in the silicon pixel. The DePMOS readout proved very low noise performance as the sensing node, buried in the silicon substrate, is coincident with the internal gate of the DePMOS transistor. DSSC foresees hexagonal pixels of 200 µm with a large SRAM that can store 640 words (9 bit) per bunch train. The ASIC, bump-bonded to the silicon sensor, performs readout, digitization and storage of the samples within the available 220 ns between the pulses.

The X-ray Active Pixel Sensor (XAMPS) is a HPD designed for protein crystallography with synchrotron radiation and now tailored for the Linear Coherent Light Source (LCLS). The new design was specifically developed for the X-ray Pump Probe instrument at LCLS [10]. The XAMPS is made on high resistivity n-type silicon and consists of a pixel array detector with integrated JFET switches. During charge integration the switches are open and then selectively closed to allow charge flow to the readout lines. Pixels are arranged in a matrix fashion which allow parallel readout of all the pixels in the same row. XAMPS is meant to provide millisecond readout, pixel size of 90 µm, input dynamic range on the order of 10^4 photons of 8 keV and a resolution of half a photon FWHM.

In the last years a number of developments of Monolithic Active Pixel Sensors (MAPS) for scientific applications have been designed and tested [11]. Given the thin active silicon layer in order to reach acceptable efficiency for X-ray energies coupling with a scintillation layer is required. Small pixel size can be achieved (e.g. 20 μm or smaller) and MAPS may feature multiple storage in-pixel so that it is capable in principle of frame rates up to several MHz [12].

The feasibility of the approaches as well as the advantages and disadvantages of different detector technologies and architectures need to be evaluated in the next months. Detectors for day-one operation should be decided both on the base of the available performances achievable with proven technologies and with novel development programs where a step in sensor performance is necessary to fulfill the requirements of the experimental cases. A balanced detector development program should therefore follow a matrix approach between the different types of detectors and the foreseen scientific experiments, with high degree of cross-fertilization, in order that the developed detectors will fulfill the scientific requirements avoiding unnecessary duplication.
Dedicated studies should also be undertaken for the development of detectors for the experiments foreseen at the Compton source, which will provide X-rays up to 1 MeV, by evaluating dedicated detector technologies and architectures.
Several other open issues like radiation hardness, medium term stability (e.g. temperature, bias voltage and charge effects), as well as calibration and data acquisition, not analyzed here for brevity, should be careful taken into account at an early stage in any detector development.
Finally a strong link to other FEL machines should also be established in order to exchange detector technologies and in order to have access to beam time at the already active facilities which will be an important test bench for the IRIDE detection systems.

References

[1] P. Lechner, et al. , Silicon drift detectors for high resolution, high count rate x-ray spectroscopy at room temperature, International Centre for Diffraction Data 2004, Advances in X-ray Analysis, Volume 47, pp.53-58
[2] S. Friedrich, Cryogenic X-ray detectors for synchrotron science, J Synchrotron Radiat. 2006, 159-171
[3] L. Strüder et al. Large-format, high-speed, x-ray pn-ccds combined with electron and ion imaging spectrometers in a multipurpose chamber for experiments at 4th generation light sources. Nucl. Instr. and Meth. A, 614(3):483–496, 2010
[4] P. Denes, D. Doering, H. A. Padmore, J.P. Walder, and J. Weizeorick, A fast, direct x-ray detection charge-coupled device, Rev. Sci. Instr. 80, 083302 (2009)
[5] A. Castoldi, A. Galimberti, C. Guazzoni, P.Rehak, R. Hartmann, L.Strüder, "Multi-Linear Silicon Drift Detectors for X-ray and compton imaging", Nucl. Instr. and Meth. A, Vol. 568, No. 1, 2006, pp. 89-95
[6] H. Graafsma. Requirements for and development of 2 dimensional x-ray detectors for European x-ray free electron laser in Hamburg. J. Instr., 4:12011, 2009
[7] D. Greiffenberg, The AGIPD detector for the European XFEL, J. Instr., Vol.7, C01103, 2012

[8] M. Hart, et al., Development of the LPD, a High Dynamic Range Pixel Detector for the European XFEL, 2012 IEEE Nuclear Science Symposium Conference Record, 2012 IEEE, Oct. 29 – Nov. 3, 2012, Anaheim (California), pp. 534 – 537
[9] M. Porro, et al., Development of the DEPFET Sensor with Signal Compression: a Large Format X-Ray Imager With Mega-Frame Readout Capability for the European XFEL, IEEE Trans. Nucl. Sci., Vol. 59, No. 6, Part 2, 2012, pp. 3339 – 3351
[10] G. A. Carini et al. Tests of small x-ray active matrix pixel sensor prototypes at the national synchrotron light source. J. Instr., 4:03014, 2009
[11] R.Turchetta et al., CMOS Monolithic Active Pixel Sensors MAPS: new 'eyes' for science, presented at Vertex 2004, Como, Italy, Special issue of Nucl. Instruments and Methods in Physics Research A, vol. 560, no. 1, 139–142
[12] J.J. Velthuis, P.P. Allport, G. Casse, A. Evans, R. Turchetta, G. Villani, A monolithic active pixel sensor for particle detection in 0.25μm CMOS technology, Nuclear Instruments and Methods A560 (2006) 40-43

6.3. THz source

The interest for having high-power, sub-ps pulsed radiation covering the spectral range from THz to MIR is rapidly growing, both as it is a powerful tool for investigating the behavior of matter at low energy, and as it allows for a number of possible applications spanning from medical science to security. After reviewing the state of the art of radiation production, spectral analysis, and detection, we discuss the construction at IRIDE of a beamline for the extraction of such a broad band radiation. The beamline will be based on a combination of different sources: Coherent Diffraction Radiation for broad band THz emission and an infrared undulator able to emit quasi-monocromatic radiation from THz to MIR. The dedicated THz laboratory is expected to provide outstanding new results in the field of solid state physics and biophysics.

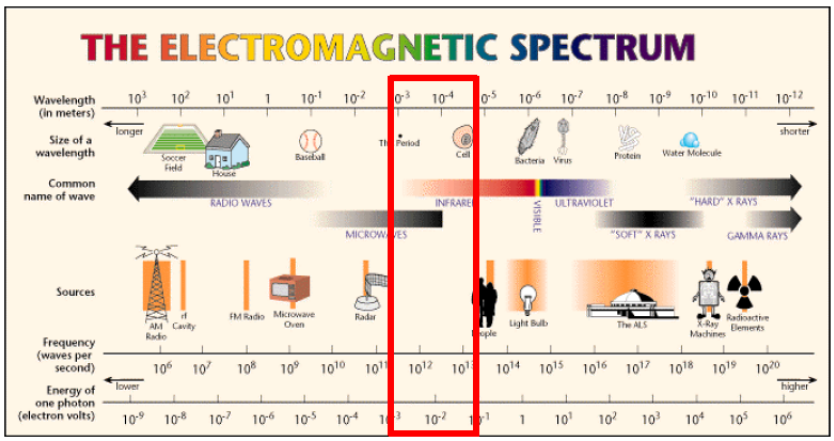

Figure 10: The electromagnetic spectrum and related sources. The red box shows the lack of available sources in the THz band.

The importance of the THz/MIR spectral range is recognized since many years, and the development of powerful and stable sources is highly requested by many fields of science: from Physics, Chemistry and Materials science to Biology, Medicine and

Security screening. During the last decade, a major effort has been devoted to fill the so-called THz gap which, see Fig. 10, resulted in a great technological improvement. Notable examples are the THz emitters [1] (photoconductive antennas, optical rectification) and quantum cascade lasers (QCL) [2].

Even if being still in a developing stage, THz spectroscopy has already displayed its potential in:

- **solid state physics**, to measure low-energy excitations like the optical gap of superconductors [3, 4] and those of the charge and spin density waves in solids [5];
- **electronics**, to directly probe the photo-excited carrier lifetime in a semiconductor, a topic of high relevance in photonics and nano-electronics;
- **biophysics,** to extract fs-resolved dynamical information on the different isomeric conformations of a given (bio-) molecule after a photo-excitation. This can be done in their native water environment [6,7]. THz/MIR spectroscopy in liquids is extremely challenging, because of the strong THz/MIR absorption of water. Its role is nevertheless crucial, since the hydrogen bonds between hydration shells and the hydrophilic and hydrophobic tails determine the tertiary structure (fold) of the proteins;
- **biological effects** of terahertz radiation [7];
- **medical imaging**, as a complementary technique to magnetic resonance;
- **security applications**, for the non-destructive detection of drugs and explosives.

Table 7: Summary of expected THz performances

Electron beam parameters	
Electron energy (GeV)	1.5 – 0.5
Charge/bunch (pC/bunch)	250
RMS bunch length (μm)	60
Normalized emittance (mm mrad)	1
Undulator	
Period (cm)	40
Number of periods	10
Magnetic field (T)	0.1 -1
Coherent Undulator Radiation parameters	
Wavelength (μm)	20 – 200
Peak power (MW)	100
Micropulse energy (mJ)	10
Micropulse duration (fs)	200
Coherent Diffraction Radiation parameters	
Wavelength (μm)	> 60
Peak power (MW)	100
Micropulse energy (μJ)	> 10
Micropulse duration (fs)	200

THz-based devices designed for security screening in the airports and in sensitive buildings are being developed in the United States and in Europe. Similarly to the Time-Domain-Spectroscopy (TDS) setup, a linac-based source can deliver broadband THz

pulses with femtosecond shaping, but with the possibility to store much more energy in a single pulse and to extend the emission up to mid-IR spectral region. One has therefore a double advantage:

i) the high peak energy (≈ mJ/pulse) and the associated electric and magnetic field in the focus (≈ 1 MV/cm and 1 Tesla, respectively), can be used to trigger new non-linear phenomena in matter. Radiation pulses from a linac-based source, at strong variance with conventional table-top generators, can then be used as a pump beam. This provides a unique chance to realize THz-pump/THz-probe and THz-MIR-pump/THz-MIR-probe spectroscopy, a technique practically unexplored up to now;

ii) one can perform time-resolved out-of equilibrium studies in the THz range on systems sensitive to heat, as it is often the case for biomaterials.

Based on the experience gained at SPARC [8,9], we propose to build a beamline collecting radiation from THz to MIR emitted both by a diffraction target (Coherent Diffraction Radiation, CDR) [10] and an infrared undulator (Coherent Undulator Radiation, CUR) [11]. In Tab. 7 we report the performances of THz/MIR coherent radiation source, so generated, depending on beam, undulator and CDR target parameters.

References:

[1] K. Reimann, Rep. Prog. Phys. 70, 1957 (2007).
[2] B.S. Williams, Nature Photonics 1, 517 (2007).
[3] M. Ortolani, et al., Phys. Rev. Lett. 97, 097002 (2006).
[4] S. Lupi et al., Phys. Rev. B 77, 054510 (2008).
[5] A. Nucara et al., Phys. Rev. Lett. 101, 066407 (2008).
[6] S. Ebbinghaus et al., PNAS 104, 20749 (2007).
[7] G. P. Gallerano, et al., Proc. IR and MM Waves, 2004, 817.
[8] E. Chiadroni et al., Rev. of Sc. Instr., under publication.
[9] E. Chiadroni et al., Appl. Phys. Lett., accepted (Jan. 2013)
[10] M. Castellano et al., Phys. Rev. E **63**, 056501 (2001).
[11] M. Gensch et al., New IR undulator beamline at FLASH, Infr. Phys. Tech. 51 (2008), 423.

6.4. Neutron Source

A Neutron Source can be realized by photo-production sending high energy electrons on a suitable high Z target. This kind of source allows to obtain neutrons with an energy spectrum that spans over more than 9 decades of energy (from few meV up to hundred of MeV), even if most of them have energy around the nuclear equilibrium temperature of the target material (for W, it is around 1 MeV) [1].

The photo-neutron energy spectra that can be obtained from a thick Tungsten target have been estimated by Monte Carlo simulations, as a function of the energy of the primary electrons interacting trough it. The results are shown in Fig. 11.

It can be seen that, for electron energy lower than 100 MeV (the case of GELINA [2]), the only relevant mechanism of production is the GDR (Giant Dipole Resonance): neutrons are emitted from the nuclei mainly for evaporative process with average energy around 1 MeV, whilst for electron energy higher than about 1GeV an important

contribution to the neutron spectra, at high energy, is added, due to the activation of the Quasi Deuteron Effect and from the pion decay intranuclear cascade.

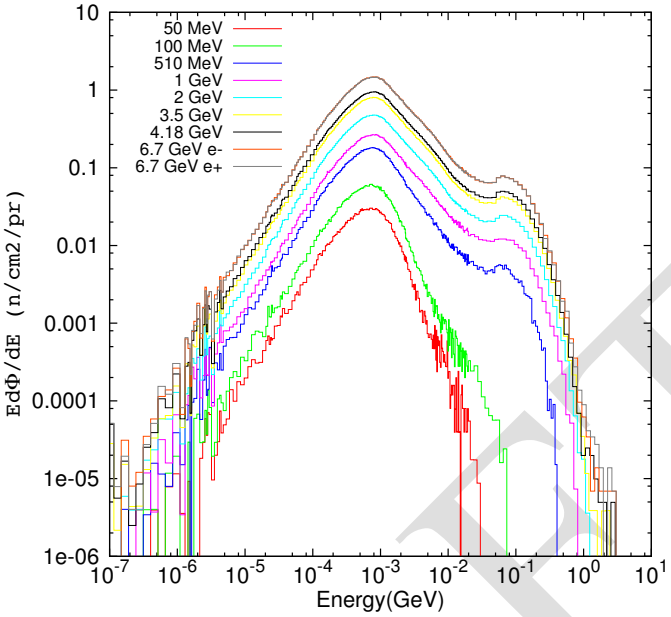

Figure 11: Neutron Spectra of neutrons emerging from W target (R=35 mm, L=60 mm), parametrised with the primary electron beam energy

A suitable design of the target, coupling neutronic and thermo-fluidodyinamic aspects, can be done in order to maximize the neutron emission rate. Preliminary and simplified analysis of the maximum neutron emission rate, in case of a thick Tungsten target and deposited power higher than a few hundreds of kW, gives a value of about 10^{15} n/s: almost an order of magnitude higher than that obtainable by GELINA.

Table 8: Expected Neutron source performances with Tungsten bulk target

Deposited Power [kW]	Primary Electron Energy [GeV]	Expected Average Neutron Emission rate [n/s]
30	1	1.3 E+14
250	1	1.0 E+15
400	1	1.7 E+15
30	3	4.3 E+13
250	3	3.3 E+14
400	3	5.6 E+14

This source may be suitable for multiple applications, ranging from material analysis for industrial and cultural heritages purposes to chip irradiation and metrology. These

applications envisage the development of properly designed beam lines with neutron moderation and possibly cold/thermal neutron transport systems. The proposed new facility will represent a great opportunity for research and development of neutron instrumentation (e.g. detectors) as well as training of young scientist in the use and development of neutron techniques.

At energies above 1 GeV and for a given thick target (i.e, able to enclose the whole electromagnetic cascade), the neutron production rate depends exclusively on the electron rate, i.e. to the ratio between power and electron energy. For a Tungsten bulk target we can estimate the performances reported in Tab. 8.

The average flux of the largest European photo-neutron facility (GELINA), to which we have to compare our predictions, is about 3E+13, but one needs to keep in mind that the solution of the thermal problems (due to the need of cooling the target) could reduce significantly the real flux respect to the rate prospected in the table.

Another relevant set of parameters is the time structure. A time structure that allows time-of-flight measurements opens a large variety of applications. Without it, significant physics is still possible.

The possible applications of a neutron beam produced with photo-production are :

Neutron Resonance Capture Analysis (**NRCA**): using pulsed epithermal neutrons (roughly below 10 keV down to 1 eV). Several elements in the periodic table show in the absorption cross section intense and relatively narrow peaks (resonances), each resonance being peculiar of the absorbing nuclide. Different isotopes of the same element may have different resonance energy. At a pulsed source the resonance are recognized as peaks in the time of flight spectrum. Each resonance is the fingerprint of a nuclear specie (isotopical recognition) thus allowing for the elemental material analysis (qualitative and quantitative) especially on metallic samples (e.g. cultural heritages). The main requirement for such measurements is the use ot the TOF technique with epithermal neutrons.

Bragg Edge Transmission (**BET**): This technique exploits the elastic (Bragg) scattering of thermal neutrons. These Bragg edges occur because, for a given *hkl* reflection, the Bragg angle increases as the wavelength increases until 2θ is equal to 180°. At wavelengths greater than this critical value no scattering by this particular *hkl* lattice spacing can occur, and there is a sharp increase in the transmitted intensity. From Bragg's law the wavelength at which this occurs is $\lambda = 2d_{hkl}$, giving a measure of the *hkl* *d*-spacing in the direction of the incoming beam. By means of this technique, stresses and strain in bulky samples can be analysed. This analysis is very important for both industrial as well as cultural heritages applications. This technique is effective using pulsed thermal neutrons and thus the TOF technique is required.

Chip irradiation: when (mostly) a high energy neutron interacts with an electronic chip, the logical state of the latter my change due to the net charge release in the active volume induced by the inelastic n-Si interaction that produce alphas and heavy ions. In complex architecture as Field Programmable Gate Array where complex algorithms can be implemented this interaction may cause the so-called Single Events Upsets (SEU) most of which are transient in nature. SEU were mostly measured using the atmospheric neutron field (produced by the primary cosmic radiation in the upper atmosphere) lasting

several months of data taking. In order to test the robustness of electronic devices to neutron field in a few minutes, neutron beams produced at facilities are desirable as the may provide an almost atmospheric-like neutron spectrum but several order of magnitude more intense. Also thermal neutrons may be responsible for SEU due to interactions (absorption) of these neutron in the boron present in electronics housing. The major application of chip irradiation are industrial ranging from aviation and aerospace (space programs), to information technologies and radiobiology. In order to perform this kind of studies atmospheric like spectra are desirable at intense fluxes. For this application TOF is not required.

Radiography and Tomography (NR, NT): Neutron Radiography exploits the attenuation of a neutron beam passing through a bulky sample. Each element absorbs neutron depending on its cross section and different isotopes of the same elements have in general different cross section. By means of radiography it is possible to obtain an image of a object that evidences the internal structure, By rotating the sample with respect to the incident beam and collecting images for each angular position a 3D image of the object is obtained (tomography). These techniques are very important for industrial (automotive and mechanical industry) as well as for cultural heritages applications. This technique is effective with cold and thermal neutrons. For this application TOF is not required.

Neutron metrology: One of the most significant features of neutron fields is the very wide range of possible neutron energies. In the nuclear industry, for example, neutrons occur with energies from those of thermal neutrons at a few meV to the upper end of the fission spectrum at perhaps 10 MeV. For cosmic ray dosimetry the energy range extends into the GeV region. This enormous range sets a challenge for designing measuring devices and a parallel challenge of developing measurement standards for characterizing these devices. Neutron standards are required from the very lowest energies, usually thermal neutrons with energies around 25 meV although so-called 'cold neutrons' with even lower energies are also produced and used at some facilities, up to neutron energies in the GeV range. These higher energies are encountered around high-energy accelerators and in the atmosphere. Neutrons produced, for example, by spallation reactions in spallation neutron sources, or in future accelerator-driven systems for the transmutation of spent nuclear fuel, will have energies ranging up to several hundred MeV. Cosmic rays from space (predominantly high- energy protons) produce neutron fields in the atmosphere with energies extending up to 10 GeV or higher.

In this context, The Italian National Institute of Ionization radiation Metrology (INMRI) is interested in having in Italy (and especially in Roma area) a high energy neutron source in order to develop primary standards for neutron emission rate and energy spectrum calibration, as required by the Italian Law No. 273/1991 and according the ISO 8529. In order to be able to assess primary standards for neutron metrology also in the high energy range, a photoneutron source obtained by very high energy electrons (1 GeV) could be interesting since it foresees to produce also neutrons above 100 MeV, even if with a rate much lower than that coming from the Giant Dipole Resonance. Finally, the accurate reconstruction of the energy spectrum from a photoneutron source is of great importance for metrological objectives with an extremely important social impact, in the frame of calibration of the ever increasing number of medial linacs, especially those used for the BNCT therapy, since these operate producing neutrons by

photoproduction on a tungsten target, in the same way as the proposed neutron source of this project. Delivering the correct dose to the cancer site, while sparing the healthy tissue, is needed for successful cancer treatments by radiation.

The beam time structure requirements are:

- **NRCA:** bunches shorter than some tens of ns and rep rate <800 Hz
- **BET:** bunches shorter than some tens of ns and rep rate <50 Hz

References

[1] R.Bedogni, L.Quintieri et al., "Experimental and numerical characterization of the neutron field produced in the n@BTF Frascati photo-neutron source", Nuclear Instruments and Methods in Physics Research A, Volume 659, 2011, p. 373-37

[2] W. Mondelaers and P. Schillebeeckx, "GELINA, a neutron time-of-flight facility for high-resolution neutron data measurements", Notiziario Neutroni e Luce di Sincrotrone, Vol. 11 n. 2 July 2006

6.5. Advanced γ-ray Compton Sources

The technology of producing γ-ray beams by Thomson/Compton back-scattering of high brightness electron beams with high energy lasers is rapidly progressing: in the last decade significant advancements in designing and commissioning Thomson sources is leading this technology to opening the Nuclear Photonics era.

Thanks to several initiatives world-wide (mainly LLNL in the US, Japan-JAEA and the European ELI-NP [1,2]) the state of the art in producing high brilliance/spectral density mono-chromatic γ-ray beams will be soon enhanced, stepping up from the present performances (γ-ray beams with bandwidth nearly 3% and spectral density of about 100 *photons/s·eV*) up to what is considered the threshold for Nuclear Photonics, *i.e.* a bandwidth of the γ-ray beam lower than 0.3% and a spectral density larger than 10^4 *photons/s·eV*. γ-ray beams of these characteristics will enable Nuclear Physics studies and Nuclear Applications based on exciting nuclear states not accessible with present machines.

The main components of a machine for Nuclear Photonics, based on a Thomson/Comtpon Source, are:

a) a high brighntess *GeV*-class electron Linac capable to deliver multi-bunch trains, *i.e.* working at 100 *Hz* rep rate with at least 50 electron bunches distributed over the RF pulse duration (from 0.5 up to 1 microsec), carrying a fraction of a *nC* bunch charge at very low rms normalized emittances (< 1 *mm·mrad*) and energy spreads (<0.1%)

b) a high energy, high quality, high rep rate laser system, delivering pulses carrying at least 1 *J* of energy (in the fundamental) with psec pulse duration at high repetition rate (100 *Hz*) with high quality (M^2<1.2), such to be focused down to typical spot sizes of 10 μm at collision with the electron bunch

c) a laser recirculator consisting of a two parabolic confocal mirror set, capable to recirculate the laser pulse a number of times equal to the electron bunches within the train (<50), by focusing it down to the collision point, recollimating and reflecting it back to

the other mirror which in turns refocuses it down back to the interaction. The recirculator should also be able to keep at any pass the quality and focusing properties of the laser pulse, properly dealing with the damaging issues on the mirror surface of such a high energy short laser pulse, and to assure an impressive precision of alignment of about 1 *μm* and 1 *μrad* over the 50 passes (with nearly 1 *m* focal length of the two mirrors).

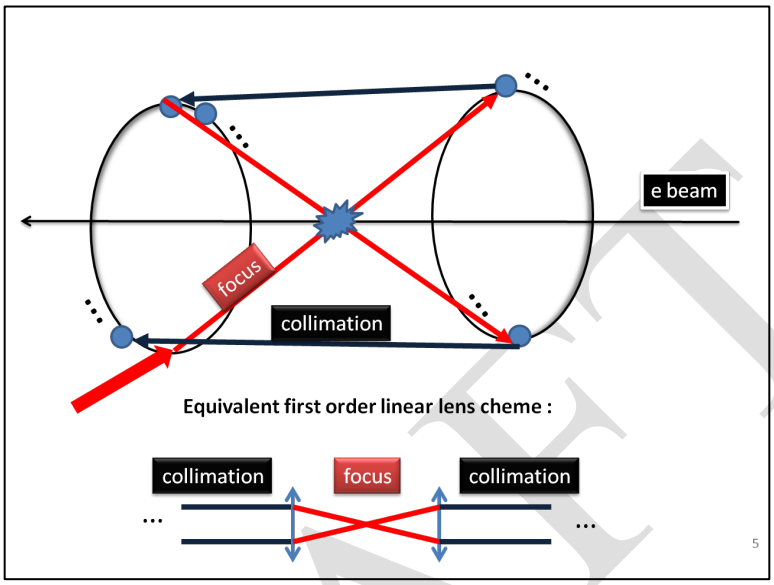

Conceptual scheme of the laser recirculator

A noticeable example of such a machine is the Egammas Source proposed by an European collaboration for the Compton Source of the ELI-NP facility. This is based on a hybrid S-band/C-band 700 *MeV* Linac, coupled to a *Ti:Sa* laser system for the collision and a laser recirculator capable of 32 passes. The expected performances for the *γ*-ray beam delivered are: tunability between 1 and 20 *MeV*, bandwidth smaller than 0.3%, full control of polarization (linear, larger than 99.8%), spectral density larger than 10^4 *photons/s·eV*, and peak brilliance larger than 10^{22} (*photons/s·mm²·mrad²·0.1%*).

Since the quality of the electron beam is largely due to the photo-injector performances, i.e. the beam dynamics in the first 120 MeV, one can conceive to integrate a full C-band photo-injector with a Superconducting Linac to boost the beam energy up to the maximum nominal value (>700 MeV), with a beam time structure and phase space quality dictated by the C-band photo-injector. Such a machine would overcome by a significant factor the *γ*-ray beam expected with the ELI-NP system. This would be achieved in conjunction with the use of a new laser technology based on *Yb:Yag* lasers, capable of an average power well above the *Ti:Sa* capability. Spectral densities up to 10^5 *photons/s·eV*, and photon fluxes up to 10^9 *photons/s* within the narrow bandwidth (0.3%) should be achievable in a well optimized and dedicated machine.

This advanced Compton source would be the fundamental brick upon which to base the portfolio of e-*γ*, *γ*-*γ* colliders foreseen in this facility. As a matter of fact, taking a larger bandwidth for the *γ*-ray beam than the one of interest for Nuclear Photonics, *i.e.* 10% vs. 0.3%, we could achieve fluxes well in excess of 10^{11} *photons/s* delivered in shots

of 10^8 *photons* per pulse, at an effective repetition rate of about 5 kHz, which is of fundamental relevance to obtain the luminosities requested by the e-γ and γ-γ colliders.

Many applications in physics require the availability of quasi-monochromatic X and γ radiation with large spectral intensity. Regarding X rays, one of their most important applications is the advanced imaging. New research techniques in the investigation of matter, which need a coherent illumination of the samples with a large flux of photons of high energy, allow to reach spatial resolutions of the order of the molecular and atomic scales and have been already used to probe nano-structured, inorganic and organic objects. Radiation at shorter wavelength, γ rays, is instead used to excite the nuclear resonant fluorescence (NRF), so that different nuclei can be identified by the distinct pattern of NRF emission peaks. Besides synchrotron radiation, free-electron lasers and high-order harmonic generation in gases, Thomson and Compton sources are among the most performing devices producing radiation with short wavelength, high power, ultra-short time duration, large transverse coherence and tunability. Existing Thomson sources have been already demonstrated to be an important tool for producing tunable quasi-monochromatic X/γ rays suitable for applications in advanced biomedical imaging and in many other fields such as crystallography, plasma, high energy, matter and nuclear physics.

In particular, Nuclear Physics will benefit from the availability of these new generation γ-ray beams for:

A) studies of the nucleus structure at the Pigmy and Giant Dipole Resonance excitation (to probe the structure and isospin properties of nuclear systems) with unprecedented resolution in reconstructing the nuclear states: this is crucial also to understand some unknown processes in the stellar nucleo-sinthesys

B) studies of two level barionc states in the high energy resonance of the nuclei, above 20 *MeV* and up to 60 *MeV*, crucial to reconstruct the equation of state of the nuclear matter

While new Nuclear Applications will be pursued thanks to these γ-ray beams in several fields:

A) detection and imaging of fissile and strategic material with isotopic reconstruction of the components (*e.g.* detection of fissile materials hidden in metallic containers), with large impact on the national security scenario

B) remote sensing and diagnosys of nuclear wastes in containers, with reconstruciotn of the isoptope and nuclear composition of the waste material, with large impact on the atomic energy scenario

C) Medical imaging and therapy

Isospin is a specific degree of freedom of the atomic nucleus: its constituents, viz. neutrons and protons, have been long recognized as members of an isospin doublet and are identified, respectively, as the tz=+1/2 and tz=-1/2 components of this doublet [WIL67]. By combining the isospin of all the constituents, one can define the isospin T of a nucleus and its components - in particular Tz which is (N-Z)/2. The nuclear Hamiltonian is (to a very good approximation) isospin-conserving, in other words

[Hnucl, T] = 0, and the nucleon-nucleon interaction is characterized by an isoscalar (T = 0) and an isovector (T = 1) part. The Coulomb interaction, plus small components of the nuclear Hamiltonian like the proton-neutron mass difference, induces an explicit symmetry breaking. This effect is also investigated at finite temperature, as reported in Ref [COR11]. The isospin symmetry is also often spontaneously broken, for instance in neutron-rich systems [PAA07].

As we discuss below, even in stable nuclei the isovector properties are poorly known: the neutron radii, the systematics of isovector collective states, the pairing interaction in the T = 0 and T = 1 channel - to name only a few - are still object of strong debate. The possibility of new experiments that clarify these issues is consequently of great importance for the development of nuclear science.

Experiments with real photons offer quite obvious advantages: the electromagnetic probes excite selectively the isovector states, and the electromagnetic interaction is well known. In addition, exclusive measurements of giant resonances providing the values of the electromagnetic and particle decays are presently very few, and are important because they are expected to provide stringent tests for theories and for the associated choice of effective interactions.

Systematics of isovector giant resonances: a nuclear Giant Resonance (GR) is a collective vibration of the nucleus that is made up with the coherent contribution of many particle-hole (p-h) excitations and exhausts a large fraction of the appropriate sum rules. When photons impinge on a nucleus, at energies around 10-20 MeV, protons feel the effect of an electromagnetic field that is oscillating in time yet is essentially constant over the nuclear volume (= hc/E ≈102 fm >> nuclear radius). Therefore, they undergo oscillations with respect to the neutrons in the nuclear center-of-mass system, in which the neutron-proton interaction acts as the restoring force. Within microscopic models like the Random Phase Approximation (RPA), that describe the resonances on the basis of single-particle (p-h) excitations [RIN80], one can obtain a microscopic picture of the collective motion and a relationship between the measurable observables and the parameters of the Hamiltonian that governs the nuclei under study.

In microscopic models the dipole spectrum displays a certain amount of fragmentation so that few states, each exhausting only part of the sum rule, show up. These states acquire a width if the coupling with more complex 2 particle-2 hole (2p-2h) configurations is taken into account; however, the fine structure remains. Consequently, exclusive experiments based on the GDR decay, together with an associated theoretical effort, would be quite important to test our basic understanding of the isovector response of nuclei and of the corresponding Hamiltonian.

Much less experimental information is available in the case of the isovector GRs having different multipolarity. Recently, using real photons available at the HIgS facility, Duke University (USA), S.S. Henshaw et al. have measured the excitation strength function of the IV giant quadrupole resonance (IVGQR) in 209Bi [HEN11]. The main IVGQR peak shows up at an excitation energy consistent with the law 135 A-1/3 and with previous measurements in the same mass region (although hadronic measurements display larger error bars). At the same time, only about 55% of the EWSR has been experimentally detected. From the theoretical side, it remains also to be tested whether these findings provide, for the IV part of the nuclear Hamiltonian, a picture which is consistent with that

extracted from the IVGDR . Experimentally, the only way to identify the IV strength is to measure the angular distribution of the γ-decay.

Relationship with the nuclear EoS: one of the open questions in nuclear physics is the determination of the equation of state, namely the relation between energy per particle and density in the nuclear medium (supposed to be uniform). From this relation one could derive the one associated with pressure vs. density, and/or extend it to finite temperature. Along a similar line as in our previous discussion, one usually distinguishes an isoscalar and isovector part of the EoS, namely one writes

$$\frac{E}{A}(\rho,\delta) = \frac{E}{A}(\rho,\delta=0) + S(\rho)\delta^2$$

in terms of the total density and of the proton-neutron asymetry $\delta = (\rho_n-\rho_p)/\rho$. The first term in the previous equation is the EoS of symmetric nuclear matter and, although still uncertain at high density, this part is certainly much better known than the second term especially around saturation. This second term defines the so-called symmetry energy S. The symmetry energy is basically unconstrained. At the same time, it is a quantity of paramount importance as it controls not only the nuclear stability but also the properties of neutron stars, the way they are formed through supernova explosion and the way they cool.

In Ref. [TRI08] an attempt has been made to extract a value of the symmetry energy at sub-saturation density (around 0.1 fm^{-3}). Moreover, in [CAR10] (based on the experimental work reported in [WIE09]) we have set a relationship between the slope of the symmetry energy at saturation, and the properties of the states appearing below the IVGDR ("pygmy" dipole resonances or PDRs). One can naturally ask the question whether other IV resonances may help constraining the symmetry energy. This question still awaits an answer. Tentatively, we could speculate that the IVGQR may probe the symmetry energy at lower densities than the IVGDR – since the power in the radial operator is larger and consequently, the peripheral part of the nuclear density is more relevant. Further investigations along this line, including searches for higher multipoles, are needed.

Decay of Giant resonances: Although a number of experimental data and theoretical studies have been cumulated, the question still exists whether we can access only the inclusive properties of the GRs (energy and fraction of exhausted sum rule), or more exclusive properties associated with the wave function of the GR. Ultimately, we can say that we still miss an unambiguous confirmation of the macroscopic picture of this collective motion. Giant resonances have a finite lifetime. Being, as a first approximation, described by coherent superposition of p-h configurations, their most probable damping mechanism is their coupling to progressively more complicated states of 2p-2h … np-nh character (up to the eventual compound nucleus state [BOR98]). This is schematically illustrated in figure below. The associated contribution to the total width, the so-called spreading width, is the dominant one. The decay width associated with the emission of one nucleon in the continuum (escape width or $\Gamma\uparrow$) is of some relevance in light nuclei but much less important in heavy nuclei. The gamma-decay width is a small fraction ($\approx 10^{-3}$) of the total width. Despite this, the study of the gamma-decay decay of GRs has been considered a valuable tool for about 30 years.

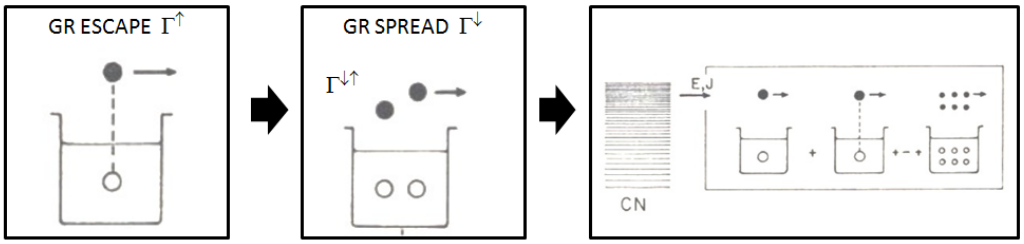

Schematic view of the process of the direct decay and damping of giant resonaces.

Recently a completely microscopic model based on Skyrme functionals has been developed. In that framework the decay of the GRs to the ground-state and low-lying excited states is calculated without any ad hoc parameter [BRE12]. For these calculations it was essential to resort to the Nuclear Field Theory (NFT) formalism, in which all the lowest-order diagrams associated with the transitions between two different RPA phonons can be consistenty calculated. It was found that, at least in the case of a particular choice for the Skyrme, the experimental result for the decay between the ISGQR of 208Pb and the 3- state can be well accounted for.

This formalism, tested for the ISGQR where data exists, is now being extended to other resonances such as the IVGDR and the IVGQR. The important question is the direct coupling to the continuum which competes with the damping into the compound nuclear states. Another question is whether the decay will enlight some fine structure of the IVGDR. Already in the pioneering experiment of Ref. [ALA91], it was pointed out that the non-statistical component of the neutron decay of the IVGDR in 208Pb, depends strongly on the IVGDR excitation energy and final state energy. The existing γ-decay calculations show that using different Skyrme interactions the IVGDR is fragmented into several peaks that do have different decay patterns.

Multiphonon states: In a quantal description of the nuclear system in terms of collective vibrations, giant resonances may be considered as one-phonon states. The existence of multiphonon states in the nuclear spectrum of excitations has been predicted since the introduction of collective models. Evidences of multiphonon states have been found in several cases but for low lying states and only fewer cases have established evidence of two phonon giant resonances. The interest in detailed exclusive studies of multiphonon states lies in answering the fundamental question: how large are the phonon-phonon interaction and anharmonicities, that is, the deviation from the harmonic boson-type excitations of a finite fermion system, such as the atomic nucleus?

The electromagnetic excitation of double giant dipole resonance states has been studied in the two nuclei ^{136}Xe and ^{208}Pb [AUM 98], via virtual photon absoption using heavy ion reactions. Only the gross features, due to the low energy resolution (few MeV) of the measurements, are known up to date and information on three- and higher-phonon states is completely lacking. High energy resolution measurements are expected to be crucial to pin down the size of the phonon-phonon interaction.

It is important to say that multi-phonon configurations can be ascribed to coherent nucleon motion manifesting density vibration in the volume or the surface of the nucleus, but subject to collisional damping mechanisms. It is quite remarkable that these states, located at much higher excitation energy than single-phonon states and thus embedded in

a continuum of uncorrelated nuclear states, appear to retain stability against decay into incoherent particle motion. The study of multi-phonon states thus allows to find evidence of coherent nucleon motion in a system presenting also the features of chaotic behaviour.
Experimental details: measurements of the gamma and particle decay of the GDR to ground states and excited states was never made using photon beams. The specifications for the gamma beams for these kind of experiments are ~100 photons at a repetition rate of ~100 MHz. The bandwidth of 0.1% sigma is ideal and unique for these measurements. One of the major difficulties is the small cross section, particularly for gamma decay with typical branching ratio of 10^{-3}. With the availability of much more intense beams with high energy resolution as those of IRIDE efforts should be made to open a new research line for the investigation of the details of giant resonances. There are in particular few cases that deserve attention. One is the gamma-gamma and particle-gamma decay from the GDR and the other is the search for multi phonon giant resonances. To address these questions gamma detection is needed. A problem to be dealt with consists to eliminate in the best possible way the gamma radiation which is produced in the target by the eletromagnetic interaction of the primary beam, which will be superimposed in our detection system to the gamma decay from specific states of the target nuclei electromagnetically excited by the gamma beam. In the case of decays, it will be important to make coincident experiments in which often one has to request the kinematical conditions such as, e.g., that the measured energy be equal to that of the impinging beam. This implies that a good time resolution is requested such as those obtainable with LaBr3:Ce scintillators (< 1 ns) [NIC07, QUA09].

References

[1] www.egammas.com

[2] www.eli-np.ro

[AUM 98] T. Aumann et al. , Ann. Rev. Nucl. Part. Sci. 48(1998)351.

[ALA91] R. Alarcon et al., Phys. Rev. C43, R2470 (1991).

[AUE83] N. Auerbach, Phys. Rep. 98, 273 (1983).

[BOR98] P.F. Bortignon, A. Bracco and R.A. Broglia, Giant Resonances. Nuclear Structure at Finite Temperature (Harwood Academic Publishers, 1998).

[BRE12] M. Brenna, G. Colò, and P.F. Bortignon, Phys. Rev. C85, 014305 (2012).

[CAR10] A. Cabone et al., Phys. Rev. C81, 041301(R) (2010).

[COR11] A.Corsi et al. PRC 84, 041304(R) (2011)

[HEN11] S.S. Henshaw et al., Phys. Rev. Lett. 107, 222501 (2011).

[NIC07] R.Nicolini et al NIM A582(2007)554–561

[QUA09] F.G.A. Quarati et al. NIMA629(2011)157–169

[PAA07] N. Paar, D. Vretenar, E. Khan, G. Colò, Rep. Prog. Phys. 70, 691 (2007).

[RIN80] P. Ring and P. Schuck, The Nuclear Many-Body Problem (Springer, New York-Berlin, 1980).

[TRI08] L. Trippa, G. Colò, and E. Vigezzi, Phys. Rev. C77, 061304(R) (2008).

[WIE09] O.Wieland et al. PRL 102, 092502 (2009).

[WIL67] D.H. Wilkinson, ed., Isospin in Nuclear Physics (North Holland, Amsterdam, 1969).

6.6. Electron-photon collider option

A high brightness linac like IRIDE could be used, in a stand alone operational mode, to drive a Compton γ−ray source, as the one discussed above. In this way γ−rays with energies of 1-100 MeV can be produced and directed head-on against electrons of 100-1000 MeV. A reach physics program can be studied [1], which includes –among others- the precise measurement of the π^0 width through the process $e\gamma \rightarrow \pi^0 e$ (*Primakoff effect*), and the search for light dark bosons in the energy region of few to hundreds MeV. These measurements, which provide important tests of the Standard Model, are not possible at present electron-photon colliders due to the low photon intensities of the machines.

π^0 width measurement: the axial anomaly of Adler, Bell and Jackiw (non-conservation of the axial vector current) is responsible for the decay of the neutral pion into two photons. It bridges in QCD the strong dynamics of infrared physics at low energies (pions) with the perturbative description in terms of quarks and gluons at high energies. The anomaly allows to gain insights into the strong interaction dynamics of QCD and has received great attention from theorists over many years. Due to the recent advances, the π^0 decay width is now predicted with a 1.4 % accuracy [2]. The major experimental information on this decay comes from the photo-production of pions on a nuclear target via the Primakoff effect [3]. The PrimEx Collaboration, using a Primakoff effect experiment at JLab, has recently achieved a 2.8 % precision [4]. This improved the PDG average for the width and mean lifetime of the pion. Nevertheless, the uncertainty of the width average is still inflated (a scale factor 1.2 at the moment), which gives an additional motivation for a new precise measurement of the pion lifetime and the two-photon decay width. The Primakoff effect-based experiments on a nucleus target suffer from model dependence due to the contamination by the coherent and incoherent conversions in the strong field of a nucleus [5]. Therefore, a measurement using a different method is highly desirable. The elecron-photon collider option is in a given sense similar to the traditional Primakoff effect setup, but provides a much cleaner environment from the theory and data analisys perspective. The proposed measurement of the pion width will have impact on the evaluation of the Standard Model prediction for the anomalous magnetic moment of the muon, a_μ. The precision of the theoretical value of a_μ is currently limited by uncertainties from the hadronic vacuum polarization and the hadronic light-by-light (HLbL) scattering contribution. The value of the latter is currently obtained using hadronic models and leads to an uncertainty in a_μ which is almost as large as the one from hadronic vacuum polarization. In view of the proposed new g-2 experiments at Fermilab and JPARC with a high precision, the HLbL contribution needs to be controlled much better, in order to fully profit from these new experiments, to test the Standard Model and to constrain the New Physics. According to model calculations, the exchange of neutral pions yields the numerically dominant contribution to the final result for HLbL scattering. The evaluation of the pion-exchange contribution has to use the normalization value (the pion decay constant) f_π. This is the same quantity, which fixes the two-photon decay width of the neutral pion. Therefore, the

precision of the π^0 width controls directly the precision of the HLbL contribution to the muon g-2.

At IRIDE we propose to use the electron-photon collisions as a source of the π^0 mesons produced via the Primakoff effect having the electron as a "target" instead of a nucleus, see Fig. 12.

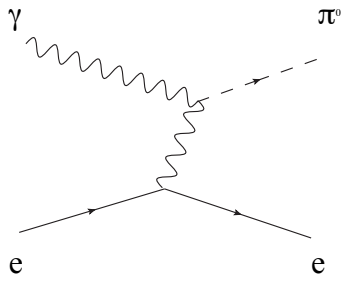

Figure 12: $e^- \gamma \rightarrow \pi^0 e^-$ diagram (*Primakoff effect*),

On the one hand, in this way one looses the Z^2 factor enhancement of the event rate; and thus the requirement for a high intensity of the photon and electron beams. On the other hand, the photon-electron collision is a much cleaner environment as compared to the photon-nucleus case. A Monte Carlo generator for the π^0 production has already been developed and we have started the simulation studies, taking into account the possible beam spread effects (at a level of 0.1% for the electron beam and 10% for the photon beam) and looking for a suitable event selection criteria. Our preliminary calculation shows that by colliding photons of 20 MeV photons against 750 MeV electrons a cross section of 1-2 nb for the process $e\gamma \rightarrow \pi^0 \gamma$ can be expected. This means that with a Luminosity of 10^{30} cm^{-2} sec^{-1} for the $e\gamma$ collider (well within reach in this proposal) a measurement of 1% is possible. This measurement would be better than the current experimental world average and the theory prediction, and competitive with the planned measurement at KLOE-2 detector, using two-photons channel [6].

Search for dark forces: several puzzling astrophysical observations (PAMELA abundance of positrons, ATIC excess, WMAP haze, INTEGRAL signal) could be explained on a common ground by existence of a new, beyond-standard-model (BSM), weakly interacting boson "U", see, e.g. [7]. The mass of the U boson is expected to be at MeV or GeV scale. Such a particle would be a slim dark matter candidate and, technically, a gauge boson of a "hidden sector" abelian symmetry group U(1), see [8]. The U boson does not interact directly with the Standard Model (SM) particles, however, it couples with the SM photon due to kinetic mixing with a tiny mixing parameter factor ε, see [9]. Therefore the SM observables mediated by a photon, would recieve a contribution from the hidden sector. The existing precision tests of SM to a high level constrain the possible range of the U boson mass and ε. Some of the SM inconsistencies can be explained by the existence of the U boson. Among the most important problems, a 3.6 sigma deviation of the muon (g-2) experiment from the SM prediction can be explained by U boson contribution, see [10]. A bulk of the parameter space for U is already excluded by various experiments, see for example a recent update of the big picture of Endo et al., [11]. However, there are numerous experimental searches for the U boson going on and planned [12].

At IRIDE we can search for U boson via the lepton triplet production process in the electron-photon collision. The main QED process of the lepton triplet production is through *u* channel exchange ("BH diagram") and the *t* channel exchange ("VCS diagram"), see Fig. 13.

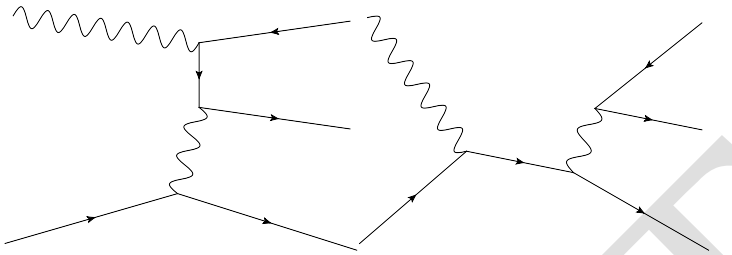

Figure 13: QED process of the lepton triplet production

The U-boson contribution is included as the *t*-channel part with the photon line modified by the mixing with the U, see Fig. 14.

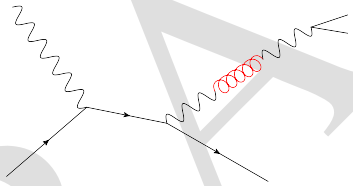

Figure 14: U-boson production (in red)

Therefore, the VCS part of the QED process is of the most importance, as it is intimately related to the U-boson production., while the BH contribution must be reduced as much as possible. This can be done by specific angular criteria for the event selection. Namely, it is foreseen that the detected electrons originated from the BH process mainly populate the region of small polar angles with respect to the beam collision axis.
We have studied the cross section integrated over whole angular region of the final particles. The results are shown in Fig. 15 for different energies of colliding beams.

As one can see, a ratio of VCS to BH contribution is decreasing when increasing the initial particle energies. In other words, the low-energy configuration is more suitable for these searches, although the U-boson mass window is reduced.

In order to find the optimized e-γ beam configuration for U boson searches, a detailed Monte Carlo simulation of the signal process and the possible QED, hadronic and machine background is in progress. To estimate the sensitivity for the U boson contribution to the cross section, one can rely on a useful relation between the QED and the U boson mediated cross section, integrated in the vicinity of the U boson resonance peak as derived by Bjorken et al. [13]. For such evaluation, one need to realistically account for the experimental resolution, which requires a detailed understanding of the detector equipment and of the analysis procedure. We have assumed a conservative detector resolution for the U mass of 5 MeV. The corresponding cross section for the U

boson with $\varepsilon \sim 10^{-3}$ is also shown in Fig. 15, which makes this search promising in the low U-mass range. In particular our results indicate an increase of sensitivity for energy-beam configuration with photons and electrons of lower energies (like ~1 MeV γ against 100 MeV e). In this case a Luminosity larger than 10^{30} cm^{-2} sec^{-1} is maybe needed.

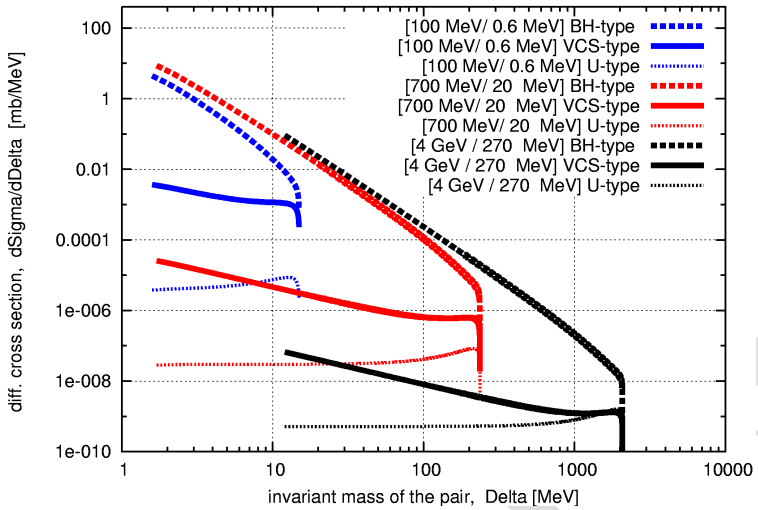

Figure 15: Differential cross section vs ee invariant mass for the process $e^- \gamma \rightarrow e^- e^+ e^-$ at different e-γ energies

Beside the precision measurement of the π^0 width and the searches for U-bosons, other physics motivations for the e-γ interaction are: the triple Compton scattering for studies of entangled states [14] and the production of μμ and ππ at rest for test of coulomb and strong effects for bound states. In any case a precision test of QED in the MeV range by e-γ interactions can be performed at IRIDE.

Although a detailed studies must be carried on, the detector required for the e-gamma interaction will be mostly made by a tracking system, a calorimeter and possibly a spectrometer in the forward direction (to detect the outcoming electrons emitted at low angle). Depending on the physics case, U boson searches or the measurement of π^0 width, the detector design could be oriented towards the one used in γγ or e^+e^- physics programs.

References:

[1] G. Venanzoni "Physics possibilities at a low energy e-γ collider" presentation at Workshop ELI-NP-GS, May 14-16, 2012
[2] Kampf, Moussallam, Phys. Rev. D 79, 076005 (2009)
[3] Primakoff, Phys.Rev. 81 (1951) 899
[4] Larin et al., Phys. Rev. Lett. 106, 162303 (2011)
[5] Kaskulov, Mosel, Phys. Rev. C 84, 065206 (2011)
[6] Eur.Phys. J. C72 (2012) 1917
[7] Arkani-Hamed et al. , Phys.Rev. D79 (2009) 015014
[8] Pospelov , Phys.Rev. D80 (2009) 095002
[9] Fayet , Phys.Rev. D75 (2007) 115017
[10] Davoudiasl, Lee and Marciano Phys.Rev.Lett. 109 (2012) 031802

[11] Phys.Rev. D86 (2012) 095029
[12] JHEP 0907 (2009) 051
[13] JHEP 0907 (2009) 051
[14] arXiv:1205.0317v1

6.7. Photon-photon collider option

The vacuum of QED poses some still unsolved challenges which are central not only in the context of field theory, but also of super-symmetry and string theory as well. The elastic photon-photon scattering offers unique opportunities to probe the nature of QED vacuum. We propose an experiment to observe photon-photon scattering in the range 1 MeV – 2 MeV CM energy, i.e., near the peak of the QED cross-section. In addition a low-energy photon-photon collider investigation could lead to the necessary technology developments and prepare the ground for a higher energy complex, while still providing a rich testing ground for QED, and, more generally, QFT.

The quantum theories of fields rank among the most spectacularly successful theories of physics, and yet they display evident shortcomings that show that we still do not understand some basic elements of the physical world. The most striking failing is the huge mismatch between the measured energy density of vacuum and the energy density of the ground level of the fundamental fields [1-3] which is wrong by something like 120 orders of magnitude. This is the so called "cosmological constant problem", and several potential solutions have been devised to get rid of it, but at the moment none of them can be considered the final one [1]. In its essence, the cosmological constant problem can be stated as follows [4]. Consider first the number of modes per unit volume of the electromagnetic (EM) field at a given frequency, which yields the energy density per unit frequency

$$u(\omega) = \frac{\hbar}{2\pi^2 c^3}\omega^3$$

then, integrating over all frequencies we find a badly divergent integral. We can select a suitable cutoff frequency, but even a mild choice like the GZK cutoff leads to huge values for the integrated energy density: in this case the energy density of the EM vacuum turns out to be about $1.6 \cdot 10^{40}$ GeV/fm^3, which is approximately 10^{41} times larger than the nuclear density (The GZK cutoff is a rough observational limit: since we observe photons with energies at least as large as the GZK cutoff, the corresponding cutoff in the integral must be equal or greater than that). Taking the Planck energy as a more natural cutoff, the energy density of the EM vacuum reaches the huge value $1.7 \cdot 10^{76}$ GeV/fm^3, which is about 120 orders of magnitude larger than the critical energy density of the universe, i.e., the energy density of a flat universe with Minkowski metric.

When we include other fields, and we note that the elementary fermionic degrees of freedom (21) give a contribution with sign opposite to that of elementary bosonic degrees of freedom (27), and we find that the problem becomes even worse. In this context Bruno Zumino noted many years ago [5] that supersymmetry – where each fermionic degree of freedom is balanced by a corresponding bosonic degree of freedom – might cure the problem, if only the threshold of supersymmetry breaking were sufficiently low.

Unfortunately, we do already know that this threshold, if it exists, is certainly much higher than required for the solution of the cosmological constant problem.
All this means that any experimental information that we may glean about the QFT vacuum is invaluable, and could bring us closer to the solution of this problem.
There are indeed a few processes that afford a direct view into QED vacuum, and photon-photon scattering is one of them. This process has no tree-level graph, and the first order contribution comes from the one-loop graph shown in Fig. 16.

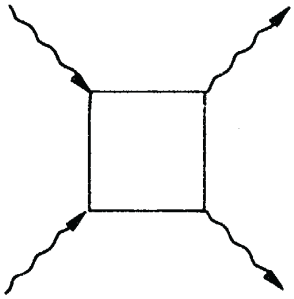

Figure 16: The basic diagram

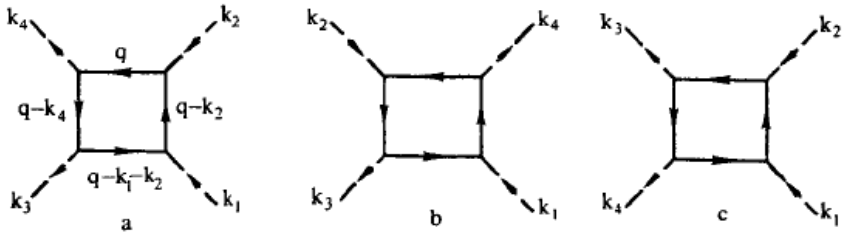

Figure 17: To compute all the scattering amplitudes we must sum over graphs with different photon indexes.

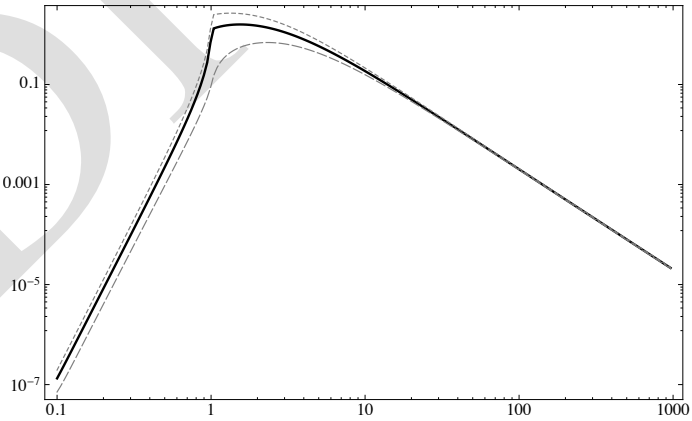

Figure 18: total cross-section (μbar) vs. CM energy (MeV). Solid line: cross-section averaged over initial photon polarizations. Dotted line: incoming photons have the same circular polarization. Dashed line: incoming photons have opposite circular polarization.

The photon-photon cross-section is directly related to the fermion loops that polarize vacuum, see Fig. 16 and Fig. 17, and therefore a photon-photon scattering experiment with photon energies in the 0.5-0.8 MeV range – where the cross-section is reasonably large, see Fig. 18 – would be an important test of our understanding of the QED vacuum.

This experiment needs a low-energy photon-photon collider, and a photon detection apparatus which is very similar to that current PET scanners. The scattered photons are rather evenly spread on the solid angle, and background from the strongly forward-backward peaked Breit-Wheeler process (pair production) is expected to be very low.

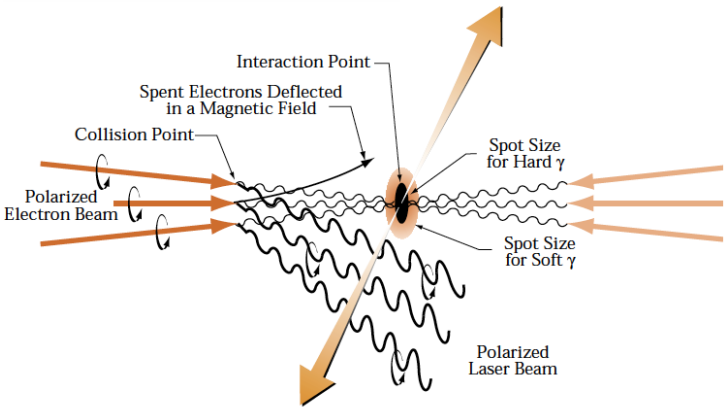

Figure 19: Scheme of principle of a photon collider. High-energy electrons scatter on laser photons and produce high-energy photon beam which collides with a similar photon or electron beam at the interaction point IP (figure taken from ref. [6]).

A low-energy photon-photon collider investigation could lead the way to the necessary technological developments and prepare the ground for a higher energy accelerator complex, while still providing a rich testing ground for QED, and, more generally, QFT.

In the case of photon-photon scattering we argue that it is important to discriminate between scatterings with different initial photon polarizations, in order to disentangle the contributions of the different matrix elements from the observed angular distribution of the scattered photons. This requirement leads to the estimate of the minimum integrated luminosity required to carry out a meaningful test.
Figure 19b shows the partially integrated differential cross-sections

$$I_{++}(\theta_1,\theta_2)=\int_0^{2\pi} d\varphi \int_{\theta_1}^{\theta_2} \sin\theta d\theta \frac{d\sigma_{++}}{d\Omega}$$

and

$$I_{+-}(\theta_1,\theta_2)=\int_0^{2\pi} d\varphi \int_{\theta_1}^{\theta_2} \sin\theta d\theta \frac{d\sigma_{+-}}{d\Omega}$$

close to the peak of the total cross-section (1.6 MeV CM energy). These partially integrated cross-sections are proportional to the number of detected photons in a PET-like

segmented detector. Their ratios are shown in figure 19.c, and each bin corresponds to a 10° azimuthal sector.

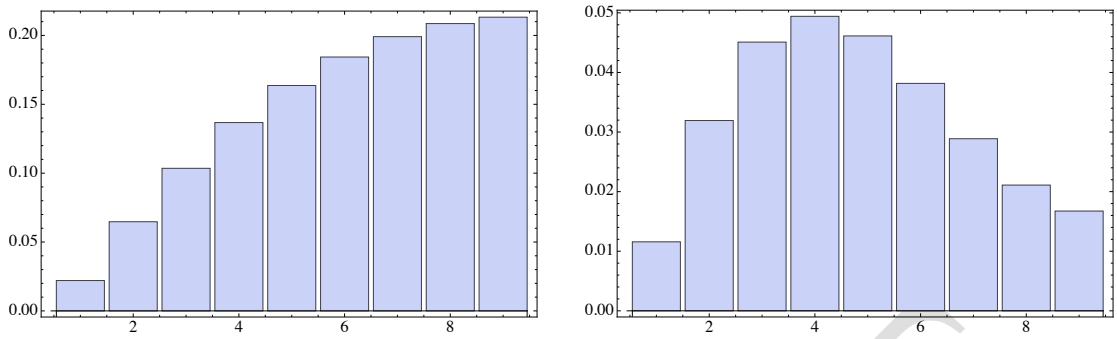

Figure 19b: Partially integrated differential cross-sections (μbarn) close to the peak of the total cross-section (1.6 MeV CM energy). Each bin corresponds to a 10° region for θ, starting from $\theta = 0°$ up to $\theta = 90°$. Left panel: partially integrated cross-section $I_{++}(\theta_1,\theta_2)$; right panel: partially integrated cross-section $I_{+-}(\theta_1,\theta_2)$.

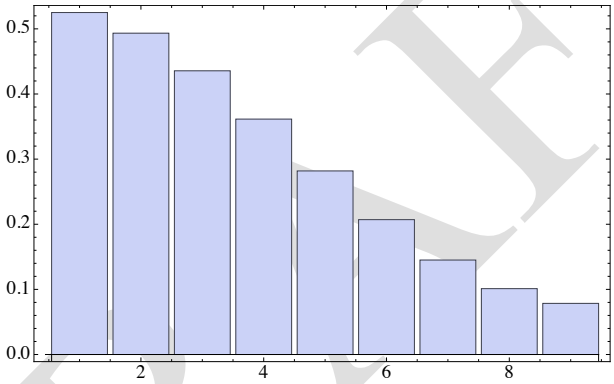

Figure 19c: Ratio $I_{+-}(\theta_1,\theta_2)/I_{++}(\theta_1,\theta_2)$ of the partially integrated differential cross-sections shown in figure 19b.

The smallest value of the ratio $I_{+-}(\theta_1,\theta_2)/I_{++}(\theta_1,\theta_2)$ is about 8%, and it occurs in the bin that spans the 80°-90° interval. This means that in order to obtain a signal-to-noise ratio of 1 in this bin, we must have an uncertainty smaller than about 8% in the determination of the number of scattering events with incoming photons that have the same circular polarization, i.e, about 170 events in the $++$ channel and about 13 events in the $+-$ channel. Since the partially integrated cross-section $I_{+-}(\theta_1,\theta_2)$ is about 0.017 μbarn in this bin, the integrated luminosity must be at least

$$\mathcal{L}\,\Delta t \geq \frac{13}{17\,\text{nbarn}} \approx 0.8\ \text{nbarn}^{-1}$$

to successfully discriminate between the cross-section over the whole angular range.
The background to $\gamma\gamma \to \gamma\gamma$ is almost exclusively due to the pair production process (Breit-Wheeler process) $\gamma\gamma \to e^+e^-$. The Breit-Wheeler process is a nuisance, however its observation will be valuable, because thus far it is still unobserved. The following table

lists the expected event rate from unpolarized initial photons (for polarized photons this rate is slightly different) and with the machine luminosity $\mathcal{L} \approx 0.8$ nbarn^{-1}s^{-1}.

Table: Background events from the Breit-Wheeler process (events/s) with unpolarized initial photons in the same angular bins specified in figures 9.5 and 9.6. Here the number of background events has been estimated for the machine luminosity $\mathcal{L} \approx 0.8$ nbarn^{-1}s^{-1}.

E_γ (MeV)	0°-10°	10°-20°	20°-30°	30°-40°	40°-50°	50°-60°	60°-70°	70°-80°	80°-90°
0.55	6.8	6.7	6.3	5.8	5.0	4.1	3.1	1.9	0.64
0.60	9.2	9.1	8.8	8.2	7.4	6.2	4.7	3.0	1.0
0.65	9.8	9.7	9.6	9.3	8.6	7.5	5.9	3.7	1.3
0.70	9.5	9.6	9.6	9.5	9.1	8.2	6.6	4.3	1.5
0.75	8.9	9.0	9.2	9.3	9.2	8.5	7.1	4.8	1.7
0.80	8.1	8.3	8.6	8.9	9.0	8.6	7.4	5.1	1.8
0.85	7.4	7.6	7.9	8.4	8.6	8.5	7.5	5.3	1.9
0.90	6.7	6.9	7.3	7.8	8.2	8.3	7.6	5.5	2.0
0.95	6.0	6.3	6.7	7.2	7.8	8.1	7.5	5.6	2.1
1.0	5.5	5.7	6.1	6.7	7.3	7.7	7.4	5.7	2.2

References

[1] S. Weinberg, Rev. Mod. Phys. **61** (1989) 1.
[2] L. Abbott, Sci. Am. 258 (1988) nr.5, 106.
[3] S. M. Carroll, W. H. Press, and E. L. Turner, Annu. Rev. Astron. Astrophys. **30** (1992) 499.
[4] R. J. Adler, B. Casey, and O. C. Jacob, Am. J. Phys. **63** (1995) 620.
[5] B. Zumino, Nucl. Phys. **B89** (1976) 535.
[6] K.-J. Kim and A. Sessler, Beamline (1996) Spring-Summer issue.

6.8. Considerations about Luminosity and Spectral density for Compton backscattering based experiments

The facility described in this document is inherently based on the conversion of beams of electrons with high brightness/phase space density into beams of high energy photons (in the *X* and γ energy range) of equivalently high brilliance/spectral density via the Thomson/Compton back-scattering mechanism.
These beams, after generation, are properly manipulated in order to set up collisions at high luminosity of different species, *i.e.* either electron-γ or γ-γ, in the range from a few MeV up to 1.5 *GeV* kinetic energy.
The energy ν_γ of the back-scattered photon is given by:

$$\nu_\gamma = \nu \frac{4\gamma^2}{1+\gamma^2\theta^2}(1-\Delta) \qquad (1)$$

where γ is the dimensionless relativistic factor of the scattering electron (whose kinetic energy is variable between a few tens of MeV and 1.5 GeV), θ is the scattering angle

(that is very small in case of head-on back-scattering between the electron beam and the laser beam), ν is the energy of the incoming laser photon (typically 1.2 *eV* for the fundamental of a *Yb:Yag* laser at 1 μm wavelength) and $\Delta = \frac{4\gamma h\nu/mc^2}{1+2\gamma h\nu/mc^2}$ is a dimensionless parameter scaling like the ratio between the incoming photon energy, as seen by the electron in its own reference system, and the electron mass energy, *i.e.* a degree of inelasticity of the back-scattering process. In our case, the maximum value for Δ is about 0.03 at 1.5 *GeV*, implying that the back-scattering process is always quasi-elastic, or, in other words is Thomson elastic scattering instead of Compton scattering. Therefore the total cross section is the well known Thomson cross section, *i.e.* 0.6 *barn*, and it does not depend on the energy of the incoming electron.
In Fig. 20 we can see the energy of the back-scattered photon as a function of the electron kinetic energy, for two different incoming laser photon: the fundamental laser wavelength (infrared at 1 μm wavelength) and the second harmonic (green light). At the maximum electron energy of 1.5 *GeV*, the photon energy is about 39 *MeV* for the fundamental and 68 *MeV* for the second harmonic ot the laser.
An important parameter to be considered, within the scenario of a multiple beam collider (e-γ, γ-γ), is the efficiency of conversion of the electron beam power into the γ-beam flux. At the end we would like to maximize the number of γ-photons produced *per electron* in the electron beam, preserving at the same time as much as possible the same phase space quality of the electron beam and mapping it into the γ-beam.

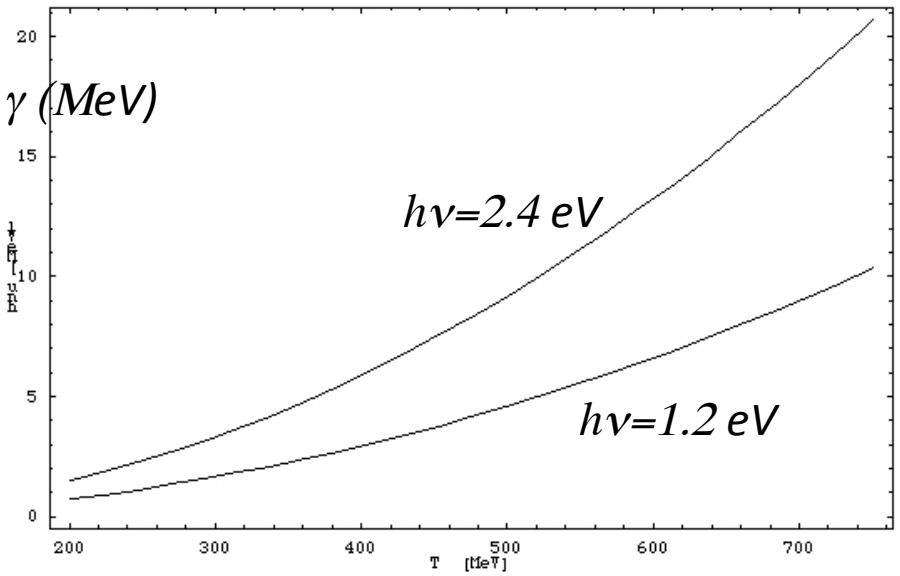

Figure 20: Energy of the back-scattered photon as a function of the electron kinetic energy, for two different incoming laser photon

The flux N_γ (photons/s) of the γ-beam is simply given by

$$N_\gamma = \Sigma_{TH} \frac{n_{el} n_{ph} f}{4\pi\sigma_{TH}^2} \qquad (2)$$

where $\Sigma_{TH} = 0.6 \cdot 10^{-24}\ cm^2$ is the Thomson cross-section, n_{el} is the number of electrons in the scattering bunch, n_{ph} is the number of photons in the incident laser pulse, f is the repetition rate of the collisions (Hz) and σ_{TH} the rms spot size of the two colliding beams at the collision point. The quantity $L_{TH} = \dfrac{n_{el} n_{ph} f}{4\pi\sigma_{TH}^2}$ is also known as the luminosity of the collision between the two beams, which gives rise to the Thomson back-scattered *X*-ray or γ-beam.

We can express N_γ also in terms of the electron bunch charge Q and the laser pulse energy U_L, getting

$$N_\gamma = 2.1 \cdot 10^8 \frac{U_L[J] Q[pC] f}{h\nu[eV]\sigma_{TH}^2[\mu m]} \tag{3}$$

It is also useful to consider the efficiency of the photon production process, which is expressed by the ratio of the number of photons generated over the number of electrons in the bunch, *i.e.* the number of photons produced *per electron*

$$n_\gamma = 34 \frac{U_L[J]}{h\nu[eV]\sigma_{TH}^2[\mu m]} \tag{4}$$

Since N_γ represents the total number of scattered photons per second over the entire solid angle and the entire energy spectrum (from the minimum energy ν up to the maximum one ν_γ, at the Compton edge), we should better consider the beam of photons which is emitted within a small solid angle and within a narrow bandwidth. The bandwidth bw scales nearly like the square of the normalized collimation angle $bw \approx \gamma^2\theta^2$, and also the number of photons emitted within the collimation angle θ has a similar scaling. So we have

$$N_\gamma^{bw} = 3.5 \cdot 10^8 \frac{U_L[J] Q[pC] f}{h\nu[eV]\sigma_{TH}^2[\mu m]} bw \quad \text{and} \quad n_\gamma^{bw} = 56 \frac{U_L[J]}{h\nu[eV]\sigma_{TH}^2[\mu m]} bw \tag{5}$$

Defining $P_{las} \equiv U_L[J] f$ as the *effective laser power available* for collisions at the interaction point, we can rewrite as

$$N_\gamma^{bw} = 3.5 \cdot 10^8 \frac{Q[pC] P_{las}}{h\nu[eV]\sigma_{TH}^2[\mu m]} bw \tag{6}$$

Assuming a collision spot size $\sigma_{TH} = 5\ \mu m$, which is almost the smallest achievable in a Thomson/Compton Source producing photons up to 20 MeV (for reasons related to the electron and laser beam quality and how they affect the γ-beam bandwidth), and considering a reasonable bandwidth $bw = 10\%$, we obtain

$$N_\gamma^{bw} = 1.2 \cdot 10^6 Q[pC] P_{las} \quad \text{and} \quad n_\gamma^{bw} = 0.19 \cdot U_L[J] \tag{7}$$

for the case of a collision laser carrying 1 μm wavelength optical photons.

In order to produce high photon fluxes N_γ^{bw} we need large collision laser powers P_{las}, while in order to achieve a good efficiency n_γ^{bw} in generating photons we need a large energy per pulse U_L.

Now let us consider two examples of Compton Sources, one based on a CW electron beam and CW Fabry-Perot laser cavity, and one based on a ELI-NP like electron beam

coupled to a laser recirculator. In order to set up the best laser and beam parameters for the two examples we need to consider the general constraints of the facility we are proposing. On one side, the *electron beam power* cannot exceed 1 *MW*, due to radio-protection and beam power limitations: this implies a maximum electron beam average current I_{av} of 1 *mA* at 1 *GeV* maximum electron energy. On the other side we consider a maximum achievable laser power in a Fabry-Perot cavity of 1 *MW* (present state of the art is nearly 100 *kW*, but many *R&D* projects are aiming at a ten-fold upgrade of the performances within the next few years). Typical Fabry-Perot cavities frequencies are around 100 *MHz* (they may be operated up to 1 *GHz* but not much below 100 *MHz*). Running at 100 *MHz* with 1 *MW* of stored power, the Fabry-Perot cavity provides laser pulses carrying 10 *mJ* at each collisions. Taking $f = 100$ *MHz* implies an electron beam carrying 10 *pC* bunch charge with 1 *mA* average current.

As far as the second example is concerned, the electron beam expected to be generated by the ELI-NP Comtpon Source is instead typical of a room-temperature RF Linac equipped with a very high beam brightness photo-injector, delivering 500 *pC* electron bunches in trains of 60 bunches, 10 *ns* spaced, at a repetition rate of the RF pulses up to 100 *Hz*. Its average current is $I_{av} = 3$ μA , implying a beam power of 3 *kW* at 1 *GeV*. The effective repetition rate of such an electron beam is $f = 6$ *kHz (60x100)*. The collision laser provides 1 *Joule* of pulse energy at a repetition rate of 100 *Hz*, that matches the repetition rate of the RF pulses feeding the accelerating sections of the Linac (for a CW SC Linac the temporal overlap is guaranteed anyway). Because each laser pulse carries about 10^{19} optical photons, of which only 10^9 per collision will be back-scattered by the electrons to become γ photons, the laser pulse is basically unperturbed by the collision, so that it can be recirculated by a proper optical device, named laser recirculator, in order to collide with all the 60 electron bunches delivered in each RF train, with a proper round-trip time that matches the 10 *ns* time separation of the electron bunches. The present ELI-NP proposal aims at 30 round-trips in the laser recirculator: we will consider an upgrade by a factor 2, as well in the electron bunch charge, which is foreseen to be 250 *pC* in the ELI-NP proposal.

We will present a comparison between these two models assuming an electron beam quality as follows: rms normalized transverse emittance $\varepsilon_n = 0.5$ μm , relative rms energy spread < 0.1%, laser rms bandwidth < 0.1% and quality $M^2 \le 1.2$, as consistent with the ELI-NP design (rms pulse duration of the electron and laser beam shorter than 1.5 *ps*).

Using eq.7 we find for the SC-CW electron beam coupled to the Fabry-Perot laser cavity:

$$N_\gamma^{bw}[SC-CW] = 1.2 \cdot 10^{13} \quad ph/s \quad \text{and} \quad n_\gamma^{bw}[SC-CW] = 0.0019 \qquad (8)$$

while for the ELI-NP beam coupled to the laser recirculator:

$$N_\gamma^{bw}[ELI-NP] = 3.6 \cdot 10^{12} \quad ph/s \quad \text{and} \quad n_\gamma^{bw}[ELI-NP] = 0.19 \qquad (9)$$

These values represent a real upper bound for the performances of a Thomson/Compton γ-beam Source. The ELI-NP case is less performant in terms of photon flux, but more efficient in terms of photon production, since we can achieve almost one γ photon produced within the bandwidth of $bw = 10\%$ every 5 incoming electrons. With an electron beam power of 3 *kW* , to be compared to 1 *MW* of the SC-CW case (which needs almost 500 electrons to produce one γ photon within the bandwidth).

Another important quantity that we need, before evaluating the luminosity of electron-γ or γ-γ collisions, is the numer of photons N_γ^{shot} produced at each collision: this is equal to $N_\gamma^{shot} \equiv N_\gamma^{bw}(f=1)$, as specified in eq.5. We have, for the two cases:

$$N_\gamma^{shot}[SC-CW] = 1.2\cdot 10^5 \quad \text{and} \quad N_\gamma^{shot}[ELI-NP] = 5.8\cdot 10^8 \qquad (10)$$

The luminosity of a γ-γ collider based on two counter-propagating γ-beams specified as in eq.8-10, is given by:

$$L_{\gamma-\gamma} = \frac{\left(N_\gamma^{shot}\right)^2 f}{4\pi\sigma_{\gamma-\gamma}^2}\ \left[cm^{-2}s^{-1}\right] \qquad (11)$$

where we keep assuming that the electron and the laser beams are round beams with equal characteristics in the horizontal and vertical planes. Furthermore, invoking that the geometrical emittance of the photon γ-beam will mimic that one of the electron beam (this is strictly true in the Thomson regime, and nearly valid in the weak Compton regime of our interest, where the electron recoil is quite small, as discussed with eq.1 when $\Delta << 1$), we can assume that the spot size at collision of the two γ-beams can be smaller than the collision spot size at the Compton interaction point. In particular, we will evaluate in the following the luminosity taking $\sigma_{\gamma-\gamma} = 1\ \mu m$, while $\sigma_{TH} = 5\ \mu m$ was used to evaluate eq. 8-10. The interaction region will have to accomodate two Compton interaction points where the two counter-propagating electron beams will collide at $\sigma_{TH} = 5\ \mu m$ with two counter-propagating laser pulses, in such a way that the focal spot-size of the two electron beams would be reached downstream the Compton interaction point at a focal spot-size value of 1 μm (as for $\sigma_{\gamma-\gamma} = 1\ \mu m$). The two γ-beams keep focusing together with the electron beams, which will have to be magnetically deflected to avoid *e-e* interactions in the γ-γ collision point. Typical distances between the two Compotn interaction points and the central γ–γ collision point is about 1 *cm* for the electron beam quality written above and the associated focal beta-function.

The luminosities for the two cases are:

$$L_{\gamma-\gamma}[SC-CW] = 1.1\cdot 10^{25} \quad \text{and} \quad L_{\gamma-\gamma}[ELI-NP] = 1.6\cdot 10^{28} \qquad (12)$$

Even in case one would like to simplify the ELI-NP-like interaction region by not implementing the laser recirculator, the luminosity would be reduced by a factor 60 (the number of round-trips), achieving $L_{\gamma-\gamma}[ELI-NP] = 2.7\cdot 10^{26}$, quite larger anyway than the SC-CW case. Since the requested integrated luminosity for the photon-photon scattering experiment is about 1 $nbarn^{-1}$, this would be reached after $6.2\cdot 10^4$ seconds of running the experiment at $L_{\gamma-\gamma} = 1.6\cdot 10^{28}$, which is equivalent to produce slightly more than one event per day.

Concerning the focusability of the electron beam and the γ-beam, we should note that achieving a 1 μm spot size at the interaction point implies a beta-function of the beams equal to $\beta^* = \frac{\gamma\sigma_{\gamma-\gamma}^2}{\varepsilon_n}$, which becomes $\beta^* = 500\ \mu m$ at $\gamma = 500$ and $\varepsilon_n = 10^{-6}\ m\cdot rad$. Since the condition $\sigma_z \le \beta^*$ must hold, to avoid the hour-glass effect (luminosity degradation due to diffraction of the two beams), we need to generate electron bunches shorter than $\sigma_z \le 500\ \mu m \approx 1.7\ ps$, which is an easy condition to fulfill with an advanced photo-injector. Assuming to run the photo-injector itself in velocity bunching

mode, we may achieve production of electron bunches down to $\sigma_z = 125\ \mu m$ with good preservation of the transverse emittance, hence allowing to reach a minimum focal spot size $\sigma_{\gamma-\gamma} = 500\ nm$ at the interaction point, which in turns would increase the luminosity by a factor 4 *w.r.t.* the values listed in eq.12.

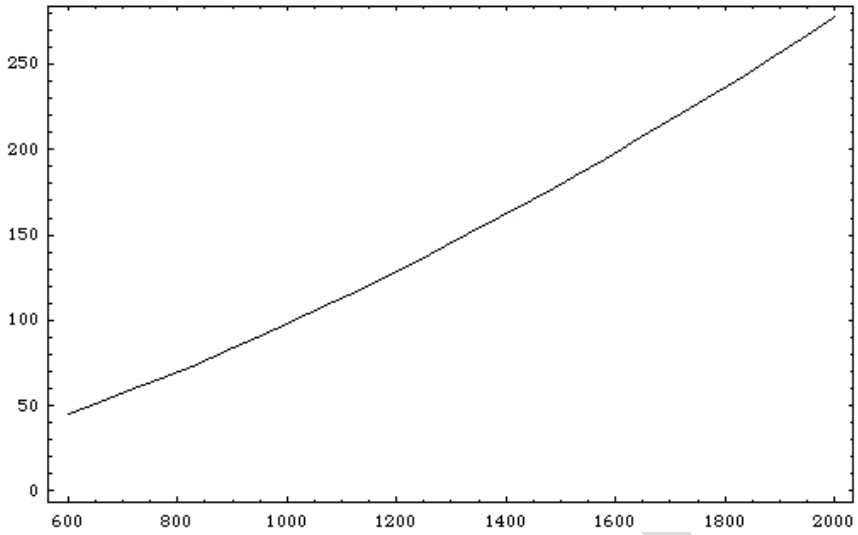

Figure 21: Energy available in the center of mass [MeV] for particle production

An electron-γ collider consists of sending an electron beam to collide with the γ-beam produced in the Thomson/Compton Source. If two independent Linacs are available, one can operate independently the electron beam producing the γ-beam from the electron beam colliding with it. In this way we can have all kind of asymmetric collisions. The energy *W* available in the center of mass for particle production is:

$$W[MeV] = 2\sqrt{T_e \cdot h\nu_\gamma} \quad ; \quad T_e = (\gamma - 1)mc^2 \tag{13}$$

Eq.13 becomes, for the Thomson/Compton Source described above (collision with a *Yb:Yag* laser) $W[MeV] = 0.003 \cdot \gamma^{3/2}$, which is plotted in Fig. 21.
As a matter of fact, with a maximum energy of 1.5 *GeV* for the electron beams (with two independent beams available), one can reach a maximum energy available for particle production of about 490 *MeV*.
The luminosity of the electron-γ collider is defined as

$$L_{e-\gamma} = \frac{n_{el} N_\gamma^{shot} f}{4\pi\sigma_{e-\gamma}^2} \left[cm^{-2}s^{-1}\right] \tag{14}$$

Noting that $n_\gamma = \frac{N_\gamma^{shot}}{n_{el}}$, we can transform eq.14 into

$$L_{e-\gamma} = \frac{L_{\gamma-\gamma}}{n_\gamma}\left(\frac{\sigma_{\gamma-\gamma}}{\sigma_{e-\gamma}}\right)^2 \tag{15}$$

We consider once again the two models of SC-CW and ELI-NP beams, for a collision performed at 1 *GeV* electron energy, in order to have *W=280 MeV*, enough for π^0 production (and the study of Primakov effect). In this case the minimum spot size we can achieve, with $\sigma_z = 125\ \mu m$ and $\varepsilon_n = 10^{-6}\ m \cdot rad$, is about $\sigma_{e-\gamma} = 250\ nm$ (note that the interaction point of the *e-γ* collider needs only one laser recirculator, reducing the complexity of the collision lay-out and interaction region, *w.r.t.* the *γ-γ* collider).

Table 9: performances of Thomson/Comtpon for the SC-CW case

Parameters for SC-CW case	**Units**	**Thomson Compton Source**	***γ-γ* collider**	***e-γ* collider**
Beam energy	[GeV]	0.1-1	0.1-1	0.1-1
Beam power	[MW]	0.1-1	0.1-1	0.1-1
Charge	[nC]	0.01	0.01	0.01
Bunch length rms	[μm]	300	300	125
Peak current	[A]	4	4	32
Rep. rate	[MHz]	100	100	100
Average current	[μA]	1000	1000	1000
rms spot size at collision	[μm]	5	1	0.25
coll. Laser eff. Power	[kW]	1000	1000	1000
coll. Laser pulse energy	[J]	0.01	0.01	0.01
rms norm. emittance	[μm]	0.5	1	1
beta-funct. at coll. (1 GeV)	[mm]	100	2	0.125
Luminosity	$cm^{-2}s^{-1}$	n.d.	$1.1\ 10^{25}$	$9.3\ 10^{28}$

Table 10: performances of Thomson/Comtpon for the ELI-NP like case

Parameters for ELI-NP case	**Units**	**Thomson Compton Source**	***γ-γ* collider**	***e-γ* collider**
Beam energy	[GeV]	0.1-1	0.1-1	0.1-1
Beam power	[MW]	< 0.003	< 0.003	< 0.003
Charge	[nC]	0.5	0.5	0.5
Bunch length rms	[μm]	300	300	125
Peak current	[A]	200	200	1600
effective Rep. rate	[Hz]	60x100	60x100	60x100
Average current	[μA]	3	3	3
rms spot size at collision	[μm]	5	1	0.25
coll. Laser eff. Power	[kW]	0.1	0.1	0.1
coll. Laser pulse energy	[J]	1	1	1
rms norm. emittance	[μm]	0.5	1	1
beta-funct. at coll. (1 GeV)	[mm]	100	2	0.125

Luminosity	$cm^{-2}s^{-1}$	n.d.	$1.6\ 10^{28}$	$1.3\ 10^{30}$

Therefore, the luminosity of the *e-γ* collider will be substantially larger than that one of the *γ-γ* collider, because the efficiency is smaller than 1 and the collision spot size is expected to be reduced by a factor 4. We have, for the two cases,

$$L_{e-\gamma}[SC-CW] = 9.3\cdot 10^{28} \quad \text{and} \quad L_{e-\gamma}[ELI-NP] = 1.3\cdot 10^{30} \qquad (16)$$

As an ultimate upgrade, the luminosity of the *e-γ* collider in the ELI-NP model, assuming to reduce the Compton collision spot size, from 5 μm down to $\sigma_{TH} = 2.5\ \mu m$, would scale up by a factor 4, which, together with a slight further upgrade of the electron bunch charge only for the electron beam colliding with the *γ*-beam (in order to avoid dilution of the *g*-beam bandwidth due to larger emittances), may push the upper limit for the luminosity to $L_{e-\gamma}[ELI-NP] = 10^{31}\ cm^{-2}s^{-1}$.

We summarize the performances of Thomson/Comtpon. Source, *γ-γ* collider and *e-γ* collider in the Tables 9 and 10, for the two models being considered.

Concerning **Nuclear Physics** performed with mono-chromatic, tunable, polarized, nicely focused *γ*-beams in the range of energy from 1 *MeV* up to several tens of *MeV* is better performed when these beams of γ photons are characterized by a large spectral density. Typical units for the Spectral Density are $photons/s\cdot eV$. Present state of the art for such *γ*-beams is the HiGS facility, in US, which is capable to deliver photons up to 8 *MeV*, bandwidths as small as 3%, spectral density nearly up to 100 $ph/s\cdot eV$.

The Eurogammas proposal for the ELI-NP Thomson/Compton Source aims at reaching a maximum energy up to 19.5 *MeV*, with a mono-chromaticity of the *γ*-beam between 0.3% and 0.5%, polarization larger than 99.5%, and spectral densities from $2\cdot 10^4\ ph/s\cdot eV$ at 1 *MeV* down to 5000 at 19.5 *MeV*.

As seen before about luminosity issues in *γ-γ* colliders, with the superconducting Linac and the Fabry-Perot laser cavity we may reach electron beams carrying 10 *pC* bunch charge with 1 *mA* average current at 100 *MHz* repetition rate, at an energy between 0.2 and 1.5 *GeV*, well suited for producing *γ*-beams from 1 to 60 *MeV*. The collision of such an electron beam with a laser pulse in a Fabry-Perot cavity supporting at 100 *MHz* a 10 *mJ* laser pulse (equivalent to 1 *MW* of stored power) will allow to reach unprecedented spectral densities and bandwidths. With *γ*-beams better suited for Nuclear Physics, carrying a few photons per pulse at high repetition rate.

The expected performances, based on the scaling laws for Thomson/Compton Sources, described before, are listed in the following Table.

One should notice that the very small bandwidth of the *γ*-beam is achieved thanks to the low emittance ε_n of the electron beam and its small energy spread $\frac{\Delta\gamma}{\gamma}$, together with a narrow bandwidth $\frac{\Delta\nu}{\nu}$ of the collision laser. The relative rms bandwidth $\frac{\Delta\nu_\gamma}{\nu_\gamma}$ of the *γ*-beam is approximately given by:

$$\frac{\Delta\nu_\gamma}{\nu_\gamma} \cong \sqrt{(\gamma\vartheta)^4 + 4\left(\frac{\Delta\gamma}{\gamma}\right)^2 + \left(\frac{\varepsilon_n}{\sigma_x}\right)^4 + \left(\frac{\Delta\nu}{\nu}\right)^2}$$

where ϑ is the collimation angle. Typically, this angle is between 200 μrad at low energy (1 *MeV*) and 40 μrad at high energy (20 *MeV*), producing a very collimated and high brilliance γ-beam which is emerging by a 10 μm wide source at very small emitting angles (as typical of X-ray beams from synchrotron radiation in undulators or FELs).

Nuclear Photonics with SC-CW e^- beam and Fabry-Perot cavity	**Units**	**Thomson Compton Source**
Beam energy	[GeV]	0.2-1.5
Beam power	[MW]	0.2-1.5
Charge	[pC]	10
Bunch length rms	[μm]	300
Rep. rate	[MHz]	100
Average current	[mA]	1
rms spot size at collision	[μm]	10
Stored Laser Power	[MW]	1
Laser pulse energy	[J]	0.01
Laser pulse rms length	[ps]	2
Laser pulse bandwidth	%	0.05
rms norm. emittance	[μm]	0.2
rms energy spread	%	0.04
Photon Peak spectrum energy	[MeV]	1-60
Phot. per shot (within bandwidth)		100
Phot. per sec (within bandwidth)		10^{10}
Rms bandwidth	%	0.1
Spectral Density @ 1 MeV	1/s·eV	10^7
Spectral Density @ 20 MeV	1/s·eV	$5 \cdot 10^5$

6.9. Electron-positron collider option

The systematic comparison of Standard Model (SM) predictions with precise experimental data served, in the last decades, as an invaluable tool to test this theory at the quantum level. It has also provided stringent constraints on "new physics" scenarios. The (so far) remarkable agreement between the measurements of the electroweak observables and their SM predictions is a striking experimental confirmation of the theory, even if there are a few cases where the agreement is not so satisfactory. On the other hand there are clear phenomenological facts (dark matter, matter-antimatter asymmetry in the universe) as well as strong theoretical arguments hinting at the presence of physics beyond the SM (bSM). The LHC, or a future e^+e^- International Linear Collider

(ILC), will hopefully answer many questions. However, their discovery potential may be substantially improved if combined with more precise low energy tests of the SM.
In this framework an electron-positron collider with luminosity of 10^{32} $cm^{-2}s^{-1}$ with center of mass energy ranging from the mass of the φ-resonance (1 GeV) up to ~3.0 GeV, would complement high-energy experiment at the LHC and future linear collider (ILC). Such a machine can easily collect an integrated luminosity of about 5 fb^{-1} in a few years of data taking, a statistics much larger than that collected at any previous machine in this energy range. This will allow one to measure the e^+e^- cross section to hadrons with a total fractional accuracy of 1%, a level of knowledge that has relevant implications for the determination of SM observables, like, the *g*-2 of the muon and the effective fine-structure constant at the M_Z scale. The latter are, through quantum effects, sensitive to possible bSM physics at scales of the order of hundred GeV or TeV.
In the following we will give a brief description of the most relevant physics issues that can be explored at this machine [1,2]. We notice that a part of this physics program, as, for instance, gamma-gamma interactions and radiative production of U vector bosons, can be pursued at an **electron – electron collider**. This option not only simplifies the layout of the machine but also presents some experimental advantages. For example in the case of gamma-gamma collisions the amount of backgrounds is considerably decreased compared to the electron-positron case.

Precision test of the Standard Model via the muon (*g-2*) - The SM determination of the anomalous magnetic moment of the muon is presently limited by the evaluation of the hadronic vacuum polarisation effects, which cannot be computed perturbatively at low energies.
The proposed machine can improve the accuracy of the leading-order hadronic contribution of the muon anomaly to about $2x10^{-10}$. This would represent a two-fold reduction of the present uncertainty, necessary to match the increased precision of the proposed muon (*g-2*) experiments at FNAL and J-PARC, and to firmly establish (or further constrain) *new physics* effects. In addition, as discussed below, there is great potential to better constrain the determination of the so-called hadronic light-by-light (LbL) contributions to (*g-2*) through measurements of photon-photon processes.

Precision test of the SM via the effective fine-structure constant at the scale M_Z - Precision tests of the Standard Model require the appropriate inclusion of higher-order effects and the knowledge of the input parameters to the best possible accuracy. One of the basic input parameters is the fine-structure constant α, determined from the anomalous magnetic moment of the electron with an impressive accuracy of 0.37 parts per billion (ppb), relying on the validity of perturbative QED. However, physics at non-zero squared momentum transfer q^2 is actually described by the effective electromagnetic coupling, the 'running' α_{em} (q^2), rather than by the low-energy constant α itself. The evolution of the fine-structure constant from the Thomson limit to higher energies involves low-energy non-perturbative hadronic effects, which spoil the precision of the determination of α at high q^2. The effective electromagnetic coupling at the scale of the Z boson, α_{em} (M_Z), is a key ingredient in the global electroweak fits of the SM. Its uncertainty affects the indirect determination of the Higgs mass already at present, and the limitations will become more severe as other parameters (like the top quark mass) are

determined ever more precisely. As measurements of the effective electroweak mixing angle at a future linear collider may improve its precision by one order of magnitude, a much better accuracy of α_{em} (M_Z) is required. By providing hadronic cross section measurements with a total fractional accuracy of 1% up to 3 GeV, we will match this request.

Photon-photon physics – The two-photon ($\gamma\gamma$) physics program (i.e., the study of the process $e^+e^- \rightarrow e^+e^- \gamma^*\gamma^* \rightarrow e^+e^-X$) gives the opportunity to investigate many aspects of the low-energy regime of QCD.
For example, studying the process of two-photon production of two pions (X = $\pi\pi$) can significantly contribute to the solution of various open questions in low-energy hadron physics. This process is a clean probe to investigate the nature of the scalar resonances. The nature of the isoscalar scalars seen in $\pi\pi$ scattering below 1.6 GeV, namely the $f_0(600)$ or σ, $f_0(980)$, $f_0(1370)$ and $f_0(1510)$ mesons, is still controversial. Various models have been proposed in which some of these states are qbar-q, some qbar-qbar-q-q, sometimes one is a Kbar-K molecule, and one a glueball, but definitive statements cannot be drawn. Their two-photon couplings will help unravelling this enigma.
Single pseudoscalar (X= π^0, η or η') production is also accessible and would improve the determination of the two-photon decay widths of these mesons, relevant for the measurement of the pseudoscalar mixing angle φ_P, and the measurement of the valence gluon content in the η' wave function. Moreover, the study of the same processes gives access to the transition form factors $F_{X\gamma^*\gamma^*}(M_X^2,Q_1^2,Q_2^2)$ at spacelike photon momentum transfer, which is relevant for the hadronic LbL scattering contributions to (g-2) of the muon. Experimental investigations of these form factors have been done so far only in the range 1 GeV^2 < Q^2 < 40 GeV^2. The region of very low Q^2 (less than 0.5 GeV^2, the more important for the LbL contributions), is devoid of experimental data and is only accessible at the DAΦNE ϕ–factory in Frascati. By increasing the energy of the machine, new higher-mass states will become accessible: pseudoscalars (like the η'), scalars (like the f_0) and axial-vector (like the a_1) mesons. A measurement of transitions form factors for these mesons will be of fundamental importance to reduce the uncertainties that currently affect the estimates of the hadronic LbL scattering.

Spectroscopy and Baryon Form Factors: cross sections of exclusive final states are also important for spectroscopy of vector mesons, whose properties provide fundamental information on interactions of light quarks. PDG lists the following vectors between 1 and 2 GeV: $\omega(1420)$, $\rho(1450)$, $\omega(1650)$, $\varphi(1680)$, and $\rho(1700)$. However, even their basic parameters (M, Γ, Γ_{ee}) are badly known. In addition many states still needed a confirmed identification. As discussed in there are still many unsolved points; some progress can be achieved in Initial State Radiation studies at BaBar and Belle, but such analyses are statistically limited, and a real breakthrough can happen at the dedicated colliders like the proposed one.
Finally, above a center-of-mass energy of $\sqrt{s} = 2m_N$ = 1.88 GeV, proton-antiproton and neutron anti-neutron pairs are produced and can be detected. The measurement of the cross-section for nucleon-antinucleon pairs allows to extract the nucleon time-like form factors. While the proton time-like form factors have been extensively measured in a wide q^2 region, the neutron time-like form factors are poorly known. More precise

information for both time-like form factors would now have an important impact on our understanding of the nucleon structure.

Searches for physics beyond the SM: Low energy, high luminosity electron-positron colliders are an ideal tool to search for hypothetical U vector bosons weakly coupled to SM particles. These bosons are predicted in extensions of the SM, which have recently appeared
in the literature as a consequence of intriguing and, as yet not completely explained, astrophysical observations. In fact, KLOE, BaBar and BES-III have already started measurements in the field. There are several possible signatures to look at, such as $e^+e^- \rightarrow e^+e^- \gamma$, $e^+e^- \rightarrow \mu^+\mu^- \gamma$, $e^+e^- \rightarrow E_{missing} + \gamma$, $e^+e^- \rightarrow E_{missing} + e^+e^- \rightarrow$, or events with four or six leptons in the final state. A careful analysis of such reactions in the region of interest for this proposal would complement the above mentioned searches, particularly in the case of the channels with missing energy or multilepton jets. The cross sections for these processes are expected to be of the order of 10-100 fb, thus one could expect to observe a few hundred events.

References:

[1] G. Venanzoni et al., "A High-Luminosity e+ e- Collider for Precision Experiments at the GeV scale", LNF - 10 / 25(IR)
[2] D. Babusci et al., "Proposal for taking data with the KLOE-2 detector at the DAΦNE collider upgraded in energy", arXiv:1007.5219

6.9.1. Considerations about electron-positron collider Luminosity

The electron-positron collider scientific case described above is based on the assumption that a luminosity of about 10^{32} $cm^{-2}s^{-1}$ can be achieved with a c.m. energy range up to 3 GeV. Certainly one of the most challenging goal of this proposal. We discuss hereafter the difficulties related to a low energy collider configuration.

Beam dynamics issues in a Linear Collider (LC) are substantially different with respect to a Circular Collider (CC) both at the Interaction Point (IP) and along the accelerating system and different is the way to optimize the luminosity [1]. Unlike a CC, in a LC the high-energy beams collide only once, and the beams must be regenerated at each pulse. In view of technological limits on the linear accelerator repetition rate, and in order to constrain the power consuption P_{AC} of the collider, the collision frequency f_{rep} is two or three orders of magnitude smaller than in a CC. Thus, to attain comparable luminosity, the LC accelerate long train of bunches and focus them to very small spot sizes.

In terms of colliding beam parameters the luminosity in a LC is defined as:

$$L = \frac{n_b N_e^2 f_{rep}}{4\pi\sigma_x^*\sigma_y^*} \times H_D = \frac{\eta_{AC} P_{AC}}{E} \times \frac{N_e}{4\pi\sigma_x^*\sigma_y^*} \times H_D = \langle I \rangle \times \frac{N_e}{4\pi\sigma_x^*\sigma_y^*} \times H_D$$

where the AC power P_{AC} to beam power $P_b = E \langle I \rangle$ conversion efficiency $\eta_{AC}=P_b/P_{AC}$ has been introduced with $\langle I \rangle = n_b N_e f_{rep}$ and:

n_b number of bunches per pulse,
N_e number of electron (positron) per bunch,
f_{rep} pulse repetition frequency,
$\sigma^*_{x,y}$ horizontal (vertical) beam size at IP,
H_D luminosity enhancement factor,
E beam energy.

As one can see from the luminosity definition at a given collision energy E and at a given operation costs represented by the available P_{AC} (in our case approximately 4 MW), there are only three apparently free parameters which can be optimized, the number of particles per bunch N_e, the beam size at the IP $\sigma^*_{x,z}$ and the luminosity enhancement factor H_D, leading to two possible approaches to a LC designs optimisation: the high beam power approach (in our case it should be limited to 1 MW) and the small beam size approach (at 1 GeV the best result has been obtained at ATF2 in Japan close to 200 nm).

The beam size at the IP is related to the beam emittance by $\sigma^* = \sqrt{\varepsilon\beta^*}$, where β^* is the betatron function at the IP, and ε is the geometrical beam emittance that depends on the whole history of the beam stability along the linac. In order to reach the required beam size at the IP, low emittance beams have to be generated and transported up to the IP. Electron sources are a mature technology in both DC and RF gun configurations. More difficult is the high quality positron beam production. Positrons can be created by pair production or by beta decay of nuclei. Pair production is the most common provider for accelerator, usually because of the desired time structure and high phase space density. A conventional positron source consists of an incident beam hitting a target, followed by focusing devices to collect the positrons before injecting in the booster linac. At present positron normalized emittance at a low energy source, are at least 2 orders of magnitude higher than the one required in our configuration. For future linear colliders positron sources based on the conversion of high energy photons have been considered. The wiggler or Compton generated photons are converted into pairs in a thin target of titanium alloy and then captured in a downstream accelerating structure. At present the only way to reach the small positron emittance values required for a LC is to inject the beam in a special storage ring, called Damping Ring (DR), when the beam energy is high enough to reduce space charge effect. Emittance reduction is achieved in a Damping Ring via the process of radiation damping, i.e. the combination of total momentum loss by synchrotron radiation emission in bending fields and longitudinal momentum gain in RF cavities, thus reducing the beam divergency. After a certain damping time an equilibrium emittance is reached determined by the damping effect and by the excitation effect arising from the statistical fluctuations in the emission of radiation quanta. A reasonable circumference of the DR has a strong impact on the time structure and length of the electron bunch train, thus limiting the potentiality of a CW SC linac.

Fortunately, because the beams are not collided again in a LC, the minimum spot size is not limited by the beam-beam tune shift as it is in CC. However the small spot sizes imposes severe constraints on the final-focus system (FFS) of the LC. The purpose of the FFS in a LC is to focus the beams to very small spot sizes required at the IP, for example in the next generation of LC, the collision spot size is measured in nanometers. In principle the FFS operates as a simple telescope. However, the strong focusing

quadrupoles that produce the small spots also generate very large chromaticities. Thus to focus a beam with a finite energy spread, the FFS must be chromatically corrected.

A primary effect of the electron-positron interaction is an enhancement of the luminosity due to the pinch effect [2], i. e. the reduction of the cross section of both beams occurring at the IP due to self focusing forces, see Fig. 22, that is included in the luminosity definition through the factor H_D. On the contrary in the case of electron-electron collisions the mutual beam forces are defocusing leading to a luminosity degradation.

The luminosity enhancement factor H_D is defined as the ratio of the luminosity L under pinch effect to the luminosity L^* when beam-beam effects are ignored:

$$H_D = \frac{L}{L^*} = \frac{\sigma_x^* \sigma_y^*}{\sigma_x \sigma_y}$$

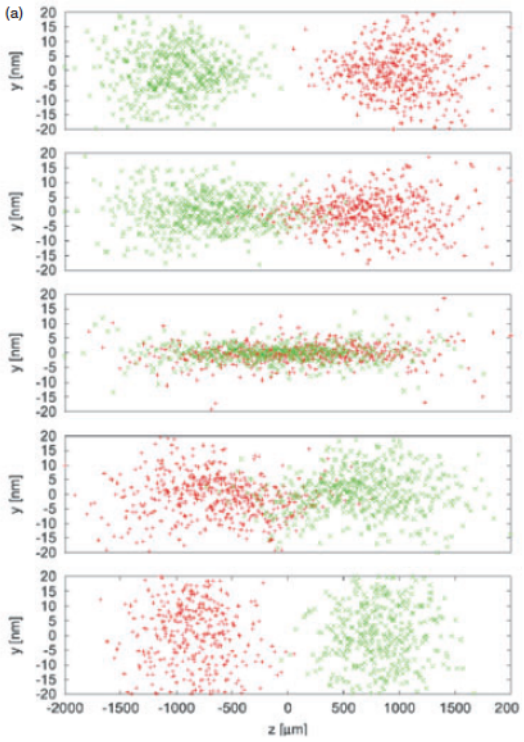

Figure 22: Pinch simulations under two different sets of initial conditions [3]. Ordinates are vertical and abscissae longitudinal particle positions, respectively, time runs downwards. The initial 'hourglass' bunch shapes reflect the β function behaviour.

The physics of the IP is rather interesting/complicated and a precise value of the enhancement factor H_D can be predicted only by computer simulations. Nevertheless some scaling law can be derived by simple arguments. When electron and positron beams are intersecting, the defocusing electrostatic force diminishes by mutual space charge neutralization and only the focusing magnetic force plays a major role as a strong attractive force between two opposite currents. A test particle that traverses a bunch of

length σ_z in the opposite direction at a distance r from the axis (impact parameter) changes its trajectory slope by $\Delta r' = -\frac{r}{f}$ as in a focusing lens, and is deflected towards the axis by $\Delta r = \Delta r' \sigma_z$. The relative change in the impact parameter is a quantity $D = \frac{\Delta r}{r} = -\frac{\sigma_z}{f}$ called disruption and is defined in terms of a Gaussian beam parameters as:

$$D_{x,y} \equiv \frac{2N_e r_e}{\gamma} \frac{\sigma_z}{\sigma_{x,y}\left(\sigma_x + \sigma_y\right)}$$

where r_e is the classical electron radius. Since the pinch reduces the area of the collision region, the luminosity is increased during the interaction and the enhancement factor scales as follows:

$$H_D = 1 + D^{1/4}\left(\frac{D^3}{1+D^3}\right)\left[\ln\left(\sqrt{D}+1\right) + 2\ln\left(\frac{0.8}{A}\right)\right]$$

where the aspect ratio parameter $A = \frac{\sigma_z}{\beta^*}$ measures the inherent divergence of the incoming beam. This is important because the natural variation of the beam size over such a distance due to the finiteness of the β function would have significant impact on the disruption process, the so called hour glass effect. Computer simulations show that maximum luminosity is achieved when particles cross over the beam axis at a distance shorter than the bunch length, i.e. $A \leq 1$. In this case each bunch emerges from the collision point with a large spread in the angles of particle trajectories and such a disrupted bunch has to be guided carefully away from the detector to minimize backgrounds. When $D > 5$ the collision process enters in the so called "pinch confinement regime": a large fraction of bunch particles is confined near the axis within a small equilibrium radius throughout the course of the interaction and the luminosity increases.

In high energy LC the benefit of luminosity enhancement is reduced by the fact that particles emit synchrotron radiation in the strong electromagnetic fields of the opposite bunch, known as "beam-strahlung". The average fractional beam energy loss due to "beam-strahlung" is approximately given by:

$$\delta_E \div \frac{r_e^3 N_e^2 \gamma}{\sigma_z\left(\sigma_x^* + \sigma_y^*\right)^2}$$

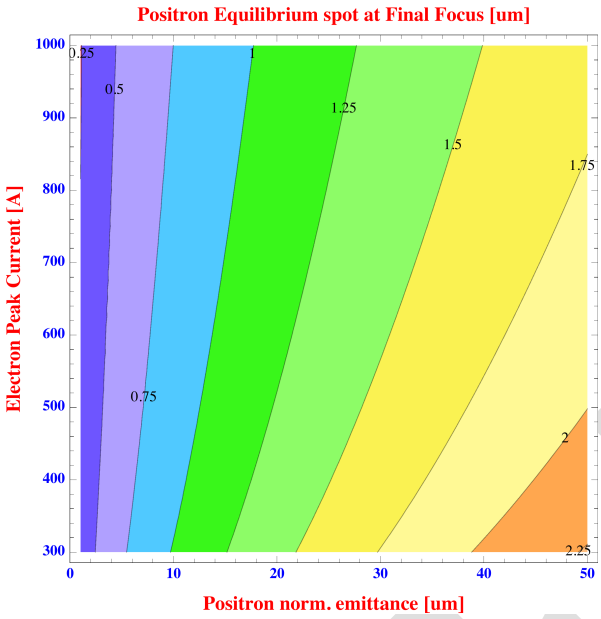

Figure 23: positron equilibrium spot size at FF versus positron beam emittance and electron peak current

Beam-strahlung leads to a large spread in the center of mass energies, reducing the accuracy during the measurement of a specific event, δ_E therefore has to be limited typically to a few percent. As reported in Tab. 11 the beam-strahlung in our case is very small thus giving us the opportunity to operate in a round beam configuration with a large disruption factor, or pinch confinement regime, with a chance to collide the beams even with a relatively relaxed positron emittance.

The required positron emittance can be evaluated by the following simple considerations. The positron beam envelope dynamics during collision can be described by the following envelope equation:

$$\sigma''_{pos,x} + \frac{k_{el}^2}{\gamma}\sigma_{pos,x} = \frac{\varepsilon_{pos,n}^2}{\gamma^2\sigma_{pos,x}^3}$$

where $k_{el}^2 = \frac{4I_{el}}{I_A\sigma_{el,x}^{*2}}$ accounts for the focusing force due to the counter-propagating electron beam current and $\sigma_{el,x}^*$ is the unperturbed electron spot size at the IP as in the case when the interaction is dominated by the positron hour glass effect, corresponding to $\beta_{el,x,y} >> \beta_{pos,x,y}$. The equilibrium solution of the previous equation is given by:

$$\sigma_{x,pos} = \sqrt[2]{\frac{\varepsilon_{n,pos}}{\sqrt{\gamma}k_{el}}}$$

Under the previous condition the positron beam spot size remains constant during the interaction due to the balance between its own defocusing emittance pressure and the counter-propagating electron beam focusing effect.

Assuming an interaction spot size of both beams of 1.5 μm at 3 GeV c.m. energy, with an electron beam peak current of 900 A the equilibrium condition is satisfied by a positron emittance lower than 35 μm, see Fig. 23. Still a challenging goal at low energy with conventional positron sources.

As an example, the parameters listed in Tab. 11 have to be obtained at the Interaction Point (IP) in order to achieve the required luminosity, assuming the SC linacs are both operating in CW mode and both electron and positron beams are round.

The third column shows the required beam parameters in the case of electron-electron collider mode. In this case the reasonable low emittance of both beams should allow operating at 500 nm spot size at IP. On the other hand the defocussing effect of colliding beam suggests operating at low charge per bunch in order to contain the luminosity degradation.

The forth column illustrate an ideal example of electron-positron collider in which both beams have the same high quality parameters. The parameters are within the state of the art for low energy electron beams but not for positrons. The fifth column shows a list of relaxed parameters for the positron beam, despite not yet state of the art, that could still results in a luminosity of 10^{32}.

Table 11: parameters at the IP of the IRIDE linear collider

Parameters	**Units**	**Electrons >< Electrons**	**Electrons >< Positrons**	**Reduced Positron quality**
Beam energy	[GeV]	1	1	1
Beam power	[MW]	1	1	0.4
AC power	[MW]	1.9	1.9	1.3
Charge	[nC]	0.2	2	0.8
Bunch length rms	[μm]	500	675	450
Peak current	[A]	120	888	533
Rep. rate	[MHz]	5	0.5	0.5
Average current	[mA]	1	1	0.4
Transverse rms spot at IR	[μm]	0.5	1.5	1.5
Norm. emittance	[μm]	1	2	10
Beta at IR	[mm]	0.5	2.6	0.45
Aspect ratio	A	1	0.3	1
Disruption parameter	D	-3.5	5.3	1.4
Beam-strahlung parameter	δ_E	$\sim 10^{-7}$	$\sim 10^{-7}$	$\sim 10^{-7}$
Luminosity enhancement factor	H_D	(<) 1	5.8	1.3
Luminosity	$cm^{-2}s^{-1}$	$\sim 2.5\ 10^{32}$	$1.6\ 10^{33}$	$\sim 1.1\ 10^{32}$

Of course a more detailed parametric optimization based on the available simulation codes should be done to understand the limits and the opportunities given by the possibility to operate in the pinch confinement regime. Moreover the positron source is still an open problem that might partially overcome by using a Damping Ring or by a new positron source concept based of direct photon conversion.

A carefully analysis of this possibilities will be the subject of a dedicated working group.

References

[1] S. Tazzari and M. Ferrario, "Trends in high energy particle accelerators", Rep. Prog. Phys. 66 1045, 2003

[2] P. Chen and K. Yokoya, "Disruption efFects from the interaction of round e+e beams", Phys Rev. D, V. 38, N. 3, 1988

[3] D. Schulte "Study of electromagnetic and Hadronic background in the TESLA IR", TESLA-Report 08, 1997

6.9.2. Considerations about Positron sources

It is interesting to explore the possibility of generating positrons by direct conversion of a gamma ray beam in a solid target [1]. There are two main advantages in this scheme:

- If the gamma photons are circularly polarized it is possible to produce a positron beam with a high degree of polarization.
- By taking advantage of a thinner target, a reduction in the opening angle of the positron beam is possible. This in conjunction with a smaller source size could bring an order of magnitude improvement to the emittance of the positron beam.

Positron production by photon conversion has *already* been shown superior to the traditional electron bombarding because the high average intensities of the beams required to maximize the collider luminosity would be otherwise seriously limited by the target damage consideration. For the same number of positron generated, a gamma ray based positron source reduces the thermal load problems because one is able to use a shorter target with lower Z material with a higher heat capacity. These advantages quantify in a two orders of magnitude increase of the thermal damage threshold in the positron production.

Conventional positron sources employ relatively thick (many radiation lengths) targets where an impinging relativistic electron beam generates positrons by Bremsstrahlung gamma-ray radiation. It is impossible to control the polarization of the Bremsstrahlung so the positron beam is not polarized. Furthermore, the thickness of the target significantly increases the source size and the angular spread of the positron beam degrading its emittance.

A 10-60 MeV gamma ray beam is required for the positron source application. In principle a 1.022 MeV photon is required to get above threshold for pair production, but

obviously the cross section increases for larger photon energies. Furthermore, the probability of the positron escaping the material increases for larger photon energy. Undulator radiation source will require a >100 GeV electron beam so this option is beyond the scope of the IRIDE project. The main possibility would be a Inverse Compton Scattering (ICS) based source using a high power 800 nm laser and a 1.5 GeV electron beam (E_e= 55 MeV).

Table 12: Comparison between Conventional and ICS positron source performances

	Conventional	**ICS based**
RMS source size	400 μm	50 μm
N. particles/driving pulse	one 600 MeV electron	one 60 MeV photon
Target thikness	$6X_0$	$0.4X_0$
RMS transverse momentum	5 MeV	1 MeV
RMS emittance	0.001 m rad	$50*10^{-6}$ m rad
N. positrons/pulse	1	0.4

There are two aspects we should examine in this novel positron source: peak and average brightness.

For the peak brightness the main advantage of driving the conversion directly with a photon beam relies on the possibility of using thinner targets. The emittance of the positron beam emerging from the target is determined by the source size and the beam divergence. The large divergence of the positrons is generated by multiple scattering in the target, while the source size is influenced by both multiple scattering and the size of the incoming electron or photon beam. Multiple scattering plays however a much stronger role in the thick target of a conventional positron source than in the thin target of a source based on the direct conversion of photons. This is the reason for the smaller divergence momentum of the positron out of a thin (0.4 radiation length) target as shown in the Tab. 12. This higher phase space density typically also helps the capture efficiency.
In terms of sources size we consider here a gamma-ray beam coming out of a Compton interaction from micron-sizes laser and electron beam. This allows the source size on the target to be < 100 μm. Assuming a gamma ray beam opening angle of $1/\gamma = 0.3$ mrad, this would imply a conversion target only 30 cm far away from the ICS focus point.
The positron yield is about 1 positron every 2 gamma ray in a 0.4 radiation length thick Ti target. The required average flux of positrons will determine the intensity of the gamma ray beam on the target and should be taken into account to estimate the total heat load. For the target, typically two atomic elements are considered: tungsten, which has a high Z = 74 and titanium, which has lower Z = 22, but better thermal conductivity characteristics.

For average power consideration it should also be noted that few joules per pulse at the collider/electron beam rep-rate are required for the laser driving the Compton

interaction. This is an issue in itself that can be addressed either by cavity recirculation schemes or by a high average power laser development (either a dedicated FEL or solid-state based).

References:

[1] K. Floettmann, "Positron Source Options for Linear Colliders", Proceedings of EPAC 2004, Lucerne, Switzerland

CONCLUSIONS

Several initiatives are being developed in the international scenario, with different aims, but with a similar underlying technology. Linear colliders with electron beams up to 500 GeV have a strong physics case, as they can be used to study the properties of the Higgs boson and to explore physics beyond the Standard Model that is not easily accessible at the LHC, even in future upgrades. At the same time there are projects aimed at producing in the next few years a new generation of machines, capable of delivering advanced beams of photons in the context of integrated facilities for multi-disciplinary research. Both initiatives are based on advanced electron Linacs.

Globally, the IRIDE infrastructure will enable new, very promising synergies between fundamental-physics-oriented research and high-social-impact applications.

As specific example the FEL radiation in the soft X-ray spectrum open possibilities for novel imaging methodologies and time-resolved studies in material science, in biology and in medicine, along with non-linear optics applications. It will allow studying crystals of size of the order of 100 nm edge outside the capability of any micro focus beam line in SR facilities with diffraction measurements of streams of nano-crystals and even of single molecules.

Another example is the high-luminosity Compton back-scattering source would be able to drive both a low-energy γ–γ collider for fundamental studies on QED, i.e. to observe and measure photon-photon scattering, and would be of great relevance to pursue strategic applications in the fields of nuclear waste diagnosis and treatment, as well as national security applications, not to mention materials science and advanced medical and radio-biological researches made possible by such a new photon source. In this way γ−rays with energies of 10-20 MeV can also be produced and directed head-on against electrons of ~700 MeV. A rich physics program can be studied, which includes – among others – the precise measurement of the π^0 width through the process $e^- \gamma \rightarrow \pi^0 e^-$ (Primakoff effect), and precision tests of QED in the MeV range. These measurements, which provide important tests of the Standard Model, are not possible at present electron-photon colliders due to the low photon intensities of the machines.

Furthermore a role of great relevance will be played by the development of dedicated X ray detectors. The signal to noise characteristics of the Silicon Drift Detectors (SDD) of large area developed by INFN and installed in the ALICE experiment at CERN-LHC have motivated a dedicated INFN project to perfection those detectors for the use in the frames of low energy X-ray detection down to energies of the order of the order of the KeV. With a process of incremental innovation those detectors, of noticeable dimensions (about 7 x 7 cm^2), are at present developed in the direction of efficient, high

resolution, reliable X-ray detection for advanced light sources. Silicon Drift Detectors in particular, because of their operation principle, are apt for the needed specific evolutionary processes.

The electron beam can also be used to produce neutrons by photo-production. The neutron spectrum produced in this way, peaked around 1 MeV, has important implications both in fundamental (nuclear X section and decay measurements) and applied physics (Neutron tomography and material studies with neutron scattering).

Powerful THz radiation sources can be also considered. The accepted paradigm of condensed matter physics n fact is that the high-energy short-time dynamics affects the low-energy long-living degrees of freedom. Actually, pushing a system out-of-equilibrium, this hierarchy could be reversed. This determines a non-linear coupling among several degrees of freedom providing the possibility to coherently manipulate different states of matter. In this scenario, one can cite for instance the possibility to coherent induce a conformation transition in macromolecules, selectively pumping a low-energy collective mode; or even inducing a coherent structural phase transition through a phonon pumping. This "low-energy" manipulation can be obtained through strong terahertz (THz) sub-ps pulses associated to electric field in the order of 1 MV/cm. Broad band THz pulses showing these characteristics can be produced in a linac by using Transition Radiation (CTR) targets or dipole radiation. Single color THz radiation, can be also produced combining a comb-beam with a CTR target. A different scheme consists in a THz ondulator which could be mount at the end of the FEL ondulators. In this case the monocromatic THz radiation could be coupled to x-ray light for THz-pump x-ray diffraction probe experiments.

Last but not least, advanced accelerators concepts could be also tested, like Plasma acceleration or Dielectric wake field acceleration, to increase the final beam energy giving new opportunities for basic and applied scientific cases.

The aim of this report was to illustrate the wide range of applications of a multi-purposes linac as the one foreseen for IRIDE. A more detailed study is under way in order to deliver a Conceptual Design Report by the end of the current year.